2016

Design and Development of a Multichannel Current-EMG System for Coherence Analysis

Comaduran Marquez, Daniel

UNIVERSITY OF CALGARY

Design and Development of a Multichannel Current-EMG System for Coherence Analysis

by

Daniel Comaduran Marquez

A THESIS

SUBMITTED TO THE FACULTY OF GRADUATE STUDIES

IN PARTIAL FULFILMENT OF THE REQUIREMENTS FOR THE

DEGREE OF MASTER OF SCIENCE

GRADUATE PROGRAM IN BIOMEDICAL ENGINEERING

CALGARY, ALBERTA

SEPTEMBER, 2016

Abstract

Electromyography (EMG), the methodology to record muscle activity, has been unchanged for many years, with the use of instrumentation amplifiers (IAs). To overcome limitations of IAs when measuring EMG activity from pennate muscles, a transimpedance amplifier (TIA) has been proposed [1]. The TIA has the advantage of conserving all frequency information in the EMG signal. However, there are some limitations of the originally proposed current-amplifier. In this thesis, we present the design and development of an improved current-amplifier. Additionally, an isolation module was developed to record from multiple muscles simultaneously. The new current-amplifier was used in two experiments. The first experiment was conducted to test coherence, a metric that determines similarity in the frequency content of two signals, as an indicator of fatigue during a dynamic activity. The second experiment was conducted to test the ability of a biofeedback system to modulate coherence.

Acknowledgements

First, I would like to thank God for giving me the opportunity to finish my master's degree, another part of the journey he has planned for me.

Second, I would like to thank the professors that guided me through this process: Dr. Nigg, Dr. Murari, Dr. von Tscharner, Dr. Herzog, and most important to Dr. Bustamante. Each one of you has taught me to be a better individual, professionally, and personally.

Third, I would like to thank my family: my wife, my parents, and my sister. Their love and support has helped me to go through the toughest moments with my chin up high, full with confidence. Everything I am today is a reflection of the love you have given me.

Last but not least, I would like to thank all the friends I made along this journey: Hossein, Isaac, Leo, Mike, Chris, Maurice, Aleen, Yuting, Lin, Kathryn, Nikhil, Colin, and many more. Without their advice and company, I would have never made it.

The following text is not just mine, but it is a collaboration of all the individuals that give my life a sense to be.

To the best family in the world: Atenea, Mom, Dad, and Pau.

Table of Contents

List of Tables

List of Figures and Illustrations

List of Symbols, Abbreviations and Nomenclature

Symbol	Definition
EMG	Electromyography
IA	Instrumentation amplifier
ADC	Analog to digital converter
AR	Autoregressive coefficient
ATP	Adenosine triphosphate
BMI	Brain-machine interface
CMR	Common mode rejection
CMRR	Common mode rejection ratio
CoI	Coherence of interest
DAQ	Data acquisition card
EEG	Electroencephalography
EKG	Electrocardiography
FFT	Fast Fourier transform
GUI	Graphical user interface
HPF	High pass filter
IC	Integrated circuit
LED	Light emitting diode
LPF	Low pass filter
MDF	Median frequency
MSC	Magnitude squared coherence
MU	Motor Unit
MUAP	Motor unit action potential
OPAMP	Operation amplifier
PCB	Printed circuit board
PSD	Power spectral density
RER	Respiratory exchange ratio
RMS	Root mean squared
SD	Standard deviation
SEM	Standard error mean
sEMG	Surface Electromyography
TCA	Transconductance amplifier
TDS	Time domain statistics
TIA	Transimpedance amplifier
VL	Vastus medialis
VM	Vastus lateralis

Chapter One: **Introduction**

The principles used to quantify electromyography (EMG) measurements have been the same for decades. The signals are acquired in either a monopolar or bipolar configuration with a high impedance differential amplifier [1]. In biomechanics, the most popular amplifier use surface electrodes with an instrumentation amplifier (IA); this methodology is known as surface EMG (sEMG) [1]. Recently, a new method to quantify muscle activity has been proposed, which relies on currents instead of potentials [2]–[5]. This new method uses a current to voltage converter, known as a transimpedance amplifier (TIA). The current-amplifier is said to be more suitable to quantify motor unit synchronization, compared to the traditional IA [2]. However, the current-amplifier has limitations related to the lack of a common mode rejection when eliminating noise from the environment. Additionally, the current-amplifier has shown to have more crosstalk issues than the conventional surface EMG when trying to measure EMG from different muscles simultaneously [5].

In the work presented here, the original EMG current-amplifier [2] has been improved with active amplification filters to maintain a steady amplification on the EMG frequencies of interest ($10 - 100\ Hz$) while diminishing signals out of that range. To eliminate the crosstalk issue, an isolation module was developed to record EMG activity with the current-amplifier from several muscles simultaneously. These design changes allow us to record a more reliable EMG signal from the current-amplifier.

The new amplifier was used to further investigate the role of frequency dependent synchronization (coherence) between selected lower limb muscles.

Additionally, a real-time coherence biofeedback system was developed to test whether lower limb coherence can be influenced by the use of such system.

1.1 Thesis objectives

Primary objective

To develop a multi-channel non-invasive current based EMG system based on the previously described technology [2].

Secondary objectives

To assess the effects of fatigue on muscular coherence between *vastus lateralis* (VL) and *vastus medialis* (VM).

To provide some initial evidence whether coherence between VL and VM muscles can be increased with the use of a biofeedback system.

1.2 Hypotheses

Hypothesis #1

Coherence between two lower limb muscles of the same functional group decreases as fatigue develops during cycling activities

Hypothesis #2

Coherence can be increased with the implementation of a biofeedback system

1.3 Thesis Outline

The thesis is presented in six chapters described as follows:

Chapter 1 describes the background of Electromyography (EMG). It presents a brief description of the current state-of-the-art for this technology. This chapter also highlights the purpose, objectives, and hypotheses of the thesis.

Chapter 2 provides a comprehensive literature review of neuromuscular physiology, EMG technology, and its limitations, it also covers the fundaments of the proposed new EMG technology. Lastly, intermuscular coherence and its importance in understanding neuromuscular control are discussed.

Chapter 3 presents the hardware design and validation of the proposed EMG technology, its fundamentals of operation and a rationale of the components selected for this project.

Chapter 4 A study to show the decrease in intermuscular coherence with fatigue during a dynamic activity is presented. The results are compared with the traditional frequency analysis of fatigue for isometric contractions.

Chapter 5 A study demonstrating voluntarily changes of intramuscular coherence using a visual biofeedback is presented.

Chapter 6 summarizes the EMG amplifier and the studies described in the previous chapters. Additionally, future directions and the general conclusions of this project are presented in this chapter.

Chapter Two: **Background**

2.1 Introduction

This chapter presents a background in electromyography (EMG), addressing the different measuring techniques and instrumentation approaches. Analysis techniques to assess muscle fatigue based on EMG measurements are also discussed. Lastly, the implementation of biofeedback systems based on EMG technology is addressed. The information in this chapter presents the background knowledge for future chapters where the role of inter-muscular EMG coherence in fatigue and biofeedback during dynamic movements is discussed.

2.2 Electromyography

EMG is an experimental technique concerned with the recording and analysis of electrical signals generated by the muscle [1]. EMG signals have been long studied because of their relationship with human movement and muscle force [6]. EMG is essential to the understanding of human movement since it illustrates the mechanisms used by the body to control the muscles. To comprehend the mechanisms of EMG we need to measure it through a sensor; to build a good sensor, we must understand what needs to be measured.

2.2.1 Physiology of EMG signal generation

2.2.1.1 Muscles

Before beginning the study of the electrical activity generated by the muscles, we need to provide a definition of the muscle. A muscle is a type of tissue that consists of long cells that

contract when stimulated and produce force[1]. Muscles can be divided into three categories as follows:

- *Smooth muscle*. It is controlled by the autonomous nervous system, thus, it is involuntarily controlled. It is called smooth because of the lack of striations, unlike the other two muscle types. It is mostly found on the walls of many internal organs (e.g. Stomach, bladder, etc.). Many of the same principles of muscle contraction from the cardiac and skeletal muscle apply to smooth muscle as well; however, its contractions tend to be much slower and last longer.
- *Cardiac muscle*. As the smooth muscle, it is an involuntary muscle. Similar in structure to skeletal muscle, however, it is only present in the heart. Its bioelectrical signals have been greatly studied to understand heart physiology. The methodology to record the electrical signals produced by this type of muscle are known as electrocardiography (EKG).
- *Skeletal muscle*. Voluntarily controlled muscle type in charge of body movement and posture maintenance. Skeletal muscles are composed of numerous chains of contractile units called muscle fibers, these fibers respond directly to neural stimuli [7]. To improve control over the fibers, a single motor nerve can activate a group containing several of these fibers. The muscle fibers are composed of myofibrils; the myofibrils contain the sarcomeres. The sarcomeres are the basic unit of the skeletal muscle, and will be further discussed.

[1] http://www.merriam-webster.com/medlineplus/muscle

2.2.1.2 Motor Unit

The nervous system is in charge of providing the commands to the muscular system to perform precise muscle contractions that allow movements. Similar to the muscles, the nervous system has a hierarchical organization [6]. A voluntary movement begins in the *premotor cortex*. The signal generated travels to the spinal cord across the pyramidal tract, passing by the basal ganglia. The basal ganglia improve and increase the precision of the desired movement; the cerebellum is then in charge of regulating the movement.

The stimuli propagate through the spinal cord until the location of the desired muscle. The signal continues its propagation to the muscle fibers through the *motor neurons*. Once the signal reaches the muscle, the signal elicits the muscle contraction initially generated by the premotor cortex. A set of muscle fibers along with their common controlling neuron and the motor nerve are called a motor unit (MU) [7].

2.2.1.3 Sarcomere

Muscle fibers are made up of small contractile units called *myofibrils*. Each myofibril exhibits an alternating pattern of dark and light bands known as *myofilaments*. Myofilaments are composed of isotropic (I) bands composed of actin filaments, and anisotropic bands (A) composed of myosin and actin filaments. The myosin filaments possess a head-like structure that creates cross-bridges with the actin filaments. These *cross-bridges* require energy in the form of adenosine triphosphate (ATP) to pull the actin filaments together generating a muscle contraction [9]. The unit between two Z lines (i.e. the disc in between the I bands) is known as a sarcomere.

2.2.1.4 Action Potential

Muscle cells are covered by a delicate elastic sheath called *sarcolemma*[2]. Under resting conditions, there is a voltage developed across the cell membrane. The resting voltage is around $-80\ mV$ from the inner side of the cell with respect to the outside [10]. This potential difference is produced by the different ionic concentrations that exist between the inner and outer part of the cell. In normal conditions (i.e. during rest) the outer part of the cell has a higher concentration of Na^+ ions compared to the inside. The opposite occurs with the K^+ ions; there is a higher concentration in the inside of the cell compared to the outside during rest.

If the muscle tissue is stimulated, an action potential occurs. First, the permeability to the Na^+ ions increase, this increases the potential of the cell to around $+30\ mV$. At the peak of the voltage, the Na^+ ion channels are closed and the K^+ channels open, letting K^+ ions outside of the cell. The release of K^+ repolarizes the membrane potential. After the repolarization, there exists a period where the cell is unable to receive another stimulus, this is known as the *refractory period*. Finally, the *sodium-potassium* pump actively (with ATP consumption) exchanges $3Na^+$ ions with $2K^+$ ions to bring the cell potential back to a resting state (Figure 2-4). Since the motorneuron innervates several muscle fibers, the activation of a motorneuron causes the activation of all the muscle fibers simultaneously. The summed electrical activity of all the muscle fibers innervated by a motorneuron is known as *motor unit action potential* (MUAP) [10].

[2] http://medical-dictionary.thefreedictionary.com/sarcolemma

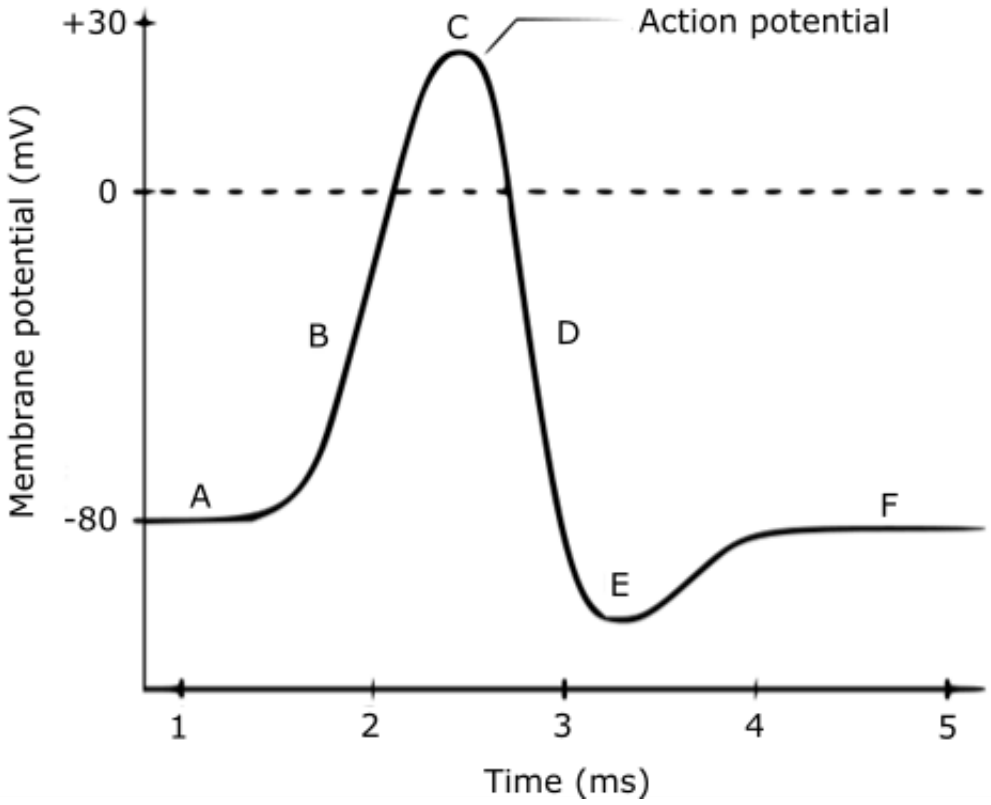

Figure 2-1. Muscle fiber action potential. (a) membrane resting potential ($-80\,mV$). (b) Depolarization, potential increases to $+30\,mV$. (c). Na^{+} channels close and the fiber cannot produce new action potentials. (d) Repolarization by the release of K^{+}. (e) Refractory period, the cell is unable to receive another stimulus. (f) Return to resting potential. [10]

2.2.2 EMG techniques

The MUAP can be recorded from the body with electronic instrumentation. Depending on the magnitude of the signal that needs to be recorded, one can select from different techniques. For the transduction of the signal, there are two techniques commonly used in the kinesiology environment [11]. These techniques vary in the type of electrode used.

2.2.2.1 Intramuscular

Also known as fine wire EMG. Intramuscular EMG consists of a needle containing two fine wire electrodes that puncture through the skin and placed into the muscular tissue. This procedure is delicate and requires proper training. Because of its complexity and invasiveness, this method may be unnecessary in some cases. However, intramuscular EMG is more suitable to record individual MU activity. This is because the electrodes sit close in proximity to the MU, therefore, the recorded activity does not suffer from energy loss through the tissue adjacent to the muscles (e.g. the skin). It is worth noting that since this method only measures electrical activity in a small portion of the muscle, it may not reflect the overall muscle activity. This is especially important in dynamic situations.

2.2.2.2 Surface

Unlike intramuscular electrodes, surface electrodes are non-invasive. Surface electrodes attach to the skin with adhesive and require a conductive solution (typically Ag or $Ag/AgCl$). Since surface electrodes are further away from the MU, the recorded signal suffers from dispersion through the adjacent tissues. This dispersion effect has to be taken into consideration when reaching any result from this kind of measurements. The skin can also be affected by the positioning of the electrodes and the relative movement of the muscle under the skin [1],

Previous studies have led some investigators to state that surface and intramuscular electrodes can provide equivalent information [12]; thus, surface EMG is preferred in kinesiology studies for being the less invasive of the two.

2.3 Electronics review

So far, we have covered the basics of how is the EMG signal generated and transduced. We will now discuss about the electronic basics to further amplify, filter, and record the EMG signal.

2.3.1 Operational Amplifiers

Operational amplifiers (OPAMPs) are among the most widely used electronic devices. They are used in many applications for consumer, industrial, and scientific devices. In this section we will describe the OPAMP function based on an ideal OPAMP. The ideal OPAMP has the following characteristics:

- Infinite open loop voltage gain
- Infinite input impedance
- Zero output impedance
- Infinite bandwidth
- Zero input offset voltage

Although the visualization of an ideal OPAMP is excellent to understand the functioning of the device, we have to keep in mind that in the real world there is no ideal OPAMP. After explaining the functioning of the ideal OPAMP, a quick review of the relevant parameters for the development of an EMG system will be discussed.

2.3.1.1 Ideal operational amplifiers

When measuring an analog signal there are two measurement types that can be performed, differential and single ended. In a single ended measurement, both the receiver and the sender

share a common ground potential. Any interference with the ground potential can contaminate the signal of interest. A differential measurement, is the measurement of the difference between two single ended measurements. Since we are measuring only the difference between both signals, any interference with the ground potential will affect both signals equally, this makes differential measurements highly immune to external interference and noise. This is known as common mode rejection (CMR).

In an ideal OPAMP, a small difference in the input generates a large difference in the output; thus, a feedback loop is often used. With the feedback, the output will change to ensure that the voltage difference between the inputs is zero. Thus, the closed loop gain can be controlled stably.

2.3.1.2 Instrumentation amplifiers

Instrumentation amplifiers (IAs) are used in many applications (e.g. automated control, data acquisition, etc.) that require the amplification of small signals. The IA is constructed from a buffered differential amplifier stage with three resistors that link in the two buffer circuits together (Figure 2-2). This configuration increases the common mode rejection ratio (CMRR) of the differential amplifiers used.

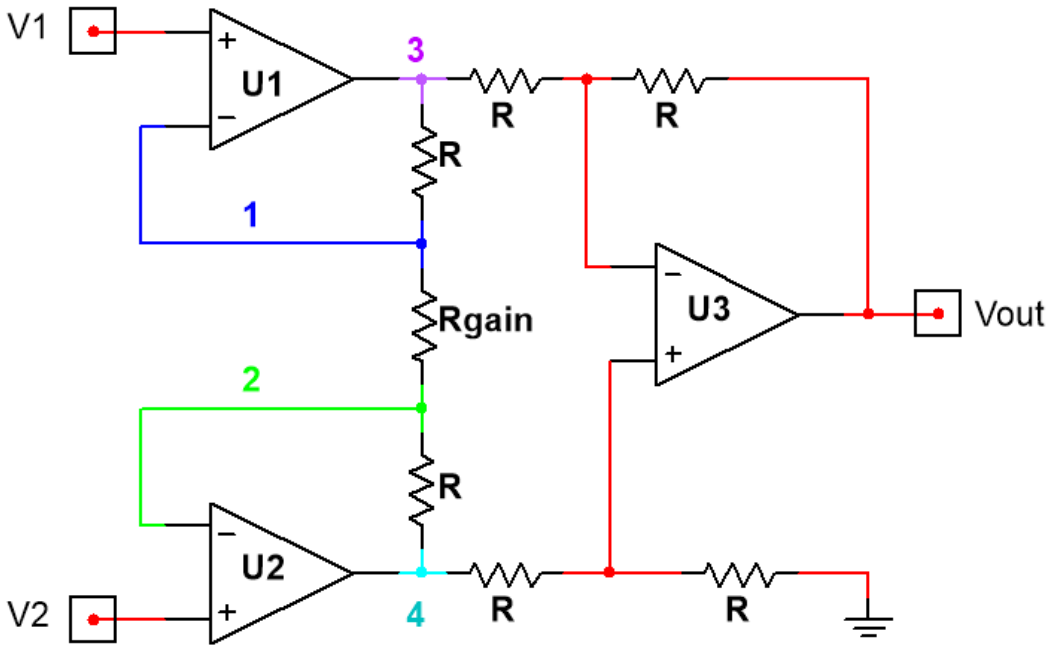

Figure 2-2. Electronic schematic of an Instrumentation Amplifier (IA).

If we consider all the resistors to be equal, except for R_{gain} the amplifier U1 will cause a voltage of V_1 at the node 1. Likewise, the node 2 will have the same voltage as V_2. This creates a voltage across R_{gain}equal to the voltage difference between V_1 and V_2. This causes a current through R_{gain}, and, since there can be no current flowing into U_1 and U_2, the current flows though the two R resistors above and below it. This causes a voltage drop as shown in equation 2.4

$$V_{3-4} = V_{1-2} * \left(1 + \frac{2R}{R_{gain}}\right) \tag{2.4}$$

The regular differential amplifier on the right of the circuit takes the voltage V_{3-4} and amplifies it with a gain of 1 (assuming that all the R resistors are equal). Manipulating equation 2.4 we have an overall voltage gain as shown in equation 2.5

$$A_v = \left(1 + \frac{2R}{R_{gain}}\right) \tag{2.5}$$

This configuration has some advantages when compared to a differential amplifier. The input OPAMPS provide a high input impedance with ease of gain adjustments through the variation of a single resistor.

2.3.1.3 Transimpedance amplifiers

The transimpedance amplifier (TIA) is also known as a current-to-voltage converter. TIAs are often used with sensors that have a current response which is more linear than a voltage response (e.g. photodiodes). As shown in Figure 2-3, the TIA consists of a feedback resistor (R_f) and capacitor (C_f). Since there is negligible current flowing to the input of the TIA, all the current goes through the R_f and C_f. The transfer function of the TIA is shown in in equation 2.6 [13].

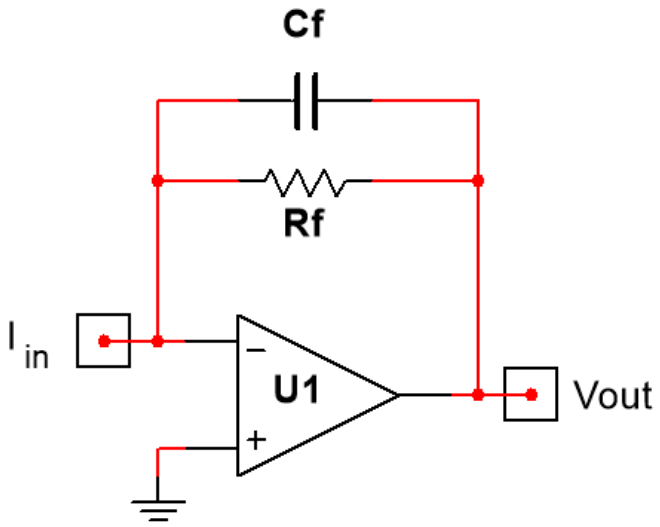

Figure 2-3. Transimpedance amplifier schematic.

$$V_{out} = \frac{-R_f}{1 + sC_f R_f} * I_{in} \tag{2.6}$$

The capacitor (C_f) will affect the frequency response of the TIA by allowing only the low frequencies to pass. The bandwidth of the TIA can be calculated with the equation 2.7. It is important to note that the TIA configuration is a single ended measurement, thus, it lacks the CMR of the IAs.

$$f_c = \frac{1}{2\pi * R_f * C_f} \tag{2.7}$$

2.3.2 Filters

A filter is a device that allows certain frequencies, or frequency ranges, to pass while it reduces other frequencies [14]. These devices are used in many scientific and engineering applications. For example, in digital acquisition systems, *antialiasing filters* are always used to ensure optimal sampling. There exist many types of filters classified on the function that they perform (e.g. notch filters, high pass, low pass, etc.). A second classification can be made based on the components of the filter (e.g. passive or active). Passive filters, also known as RLC filter, use resistors, capacitors and inductors. Active filters use OPAMPS, resistors, and capacitors. Below, a description of the most common and basic filters.

2.3.2.1 Low pass filter

In an ideal case, a low-pass filter (LPF) is a filter that only allows frequencies below a specified frequency to pass. The specified frequency is known as the cutoff frequency (f_c). This means that there are two zones for the LPF: a pass-band, and a rejection band. However, in reality,

there is no such thing as an ideal LPF. A non-ideal LPF consists of three bands: a pass-band, a transition band, and a rejection band.

LPFs can have different orders; a parameter to express how short is the transition band. Higher orders have a shorter transition band, but require more components and filtering stages. The order of the filter is the number of poles (in the case of LPFs) of the filter equation (equation 2.8).

$$G(s) = \frac{G_0}{\prod_i (1 + \alpha_i s) * \prod_j \left(1 + \alpha_j s + b_j s^2\right)} \tag{2.8}$$

Changing the parameters of the complex poles of equation 2.8, we can obtain three major filter types based on their frequency response. Figure 2-4 shows the magnitude of the frequency response of the three different LPFs.

- *Butterworth*. This filter type gives a maximum pass-band flatness
- *Tschebyscheff*. Gives a sharp transition between pass band and stopband.
- *Bessel*. Provides a linear phase response.

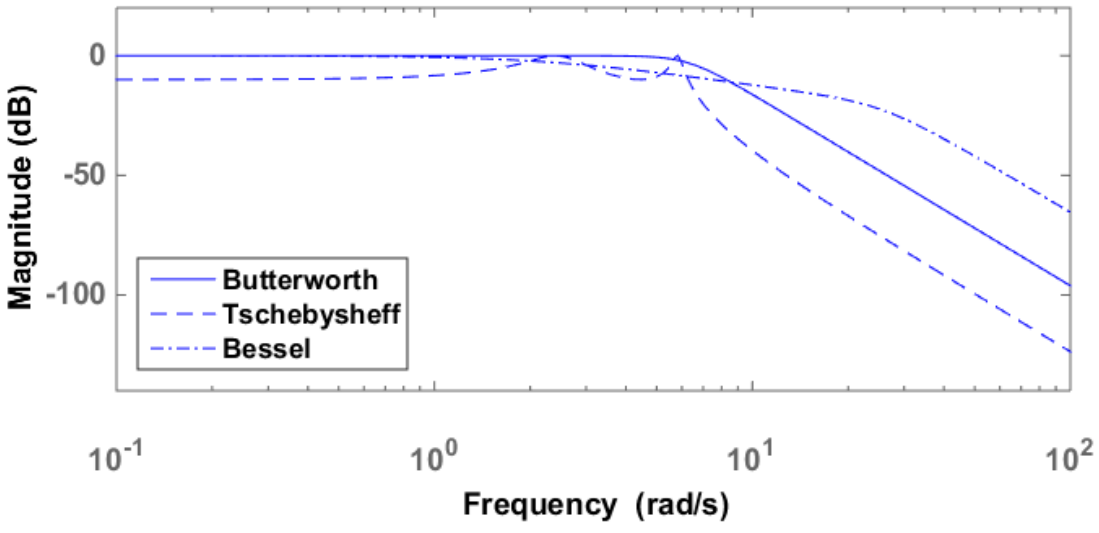

Figure 2-4. Comparison of gain responses of fourth order low pass filters.

2.3.2.2 High pass filter

The high pass filter (HPF) is the opposite of the LPF in the sense that it only allows frequencies higher than the f_c to pass. All the concepts of the LPF apply to the HPF as well. When an HPF is designed, the components chosen for a LPF are interchanged (i.e. switching resistors for capacitors and vice versa). This interchange process is known as *mirroring effect* (Figure 2-5).

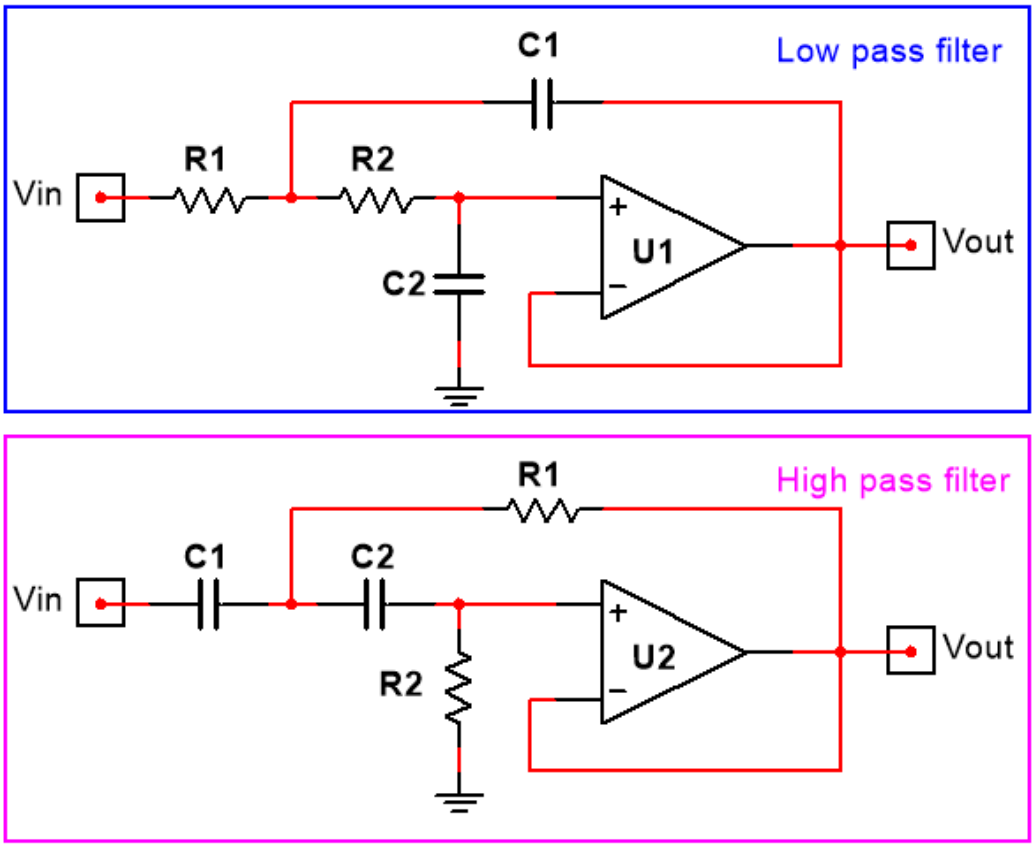

Figure 2-5. Second order LPF and HPF with Sallen key topology showing the mirroring effect.

2.3.3 Analog to digital conversion

Any analog signal that needs to be stored, processed, analyzed or displayed in a computer needs to be converted to a digital signal first. Digitalization is the representation of an object, image, sound, document, or signal that describes a discrete set of its points or samples[3]. The process of digitizing a signal is carried out by a device known as an analog-to-digital converter. The main characteristics of an analog to digital conversion are:

- *Sampling rate*, is the rate at which the discrete points of the digital signal are sampled (measured) from the continuous analog signal. Is also known as *sampling frequency*. The parameter is expressed as the quantity of discrete points sampled in a time period. A higher sampling rate takes more discrete points in a certain amount of time. The higher the sampling rate, the faster one can detect a change in the analog signal.

  The sampling rate is selected according to the Nyquist- Shannon sampling theorem. This theorem says that the sampling frequency has to be at least two times higher than the highest expected frequency in the signal in question. The frequency value that meets this requirement is known as the Nyquist frequency.
- *Aliasing*. It is defined as the misidentification of a signal frequency, introducing distortion or error[4]. It occurs when the discrete representation of two different continuous signals cannot be distinguished from one another, and it becomes impossible to reconstruct the original signal from its digital equivalent. Thus, information is lost. Since the digitization of a signal takes discrete time points, there always exist a time period where the continuous

[3] http://www.oxforddictionaries.com/us/definition/american_english/digitize
[4] http://www.oxforddictionaries.com/us/definition/american_english/aliasing

signal is not measured. If the discrete points are fast enough, one can assume that the information that was not sampled lies between those points. However, if the sampling rate is too slow, the continuous signal could take a completely different value at the moment it is not being sampled (Figure 2-6).

Anti-aliasing filters, filter the analog signal before the analog-to-digital conversion takes place. These filters avoid higher frequencies that could be sampled, thus making the sampled signal impossible to reconstruct.

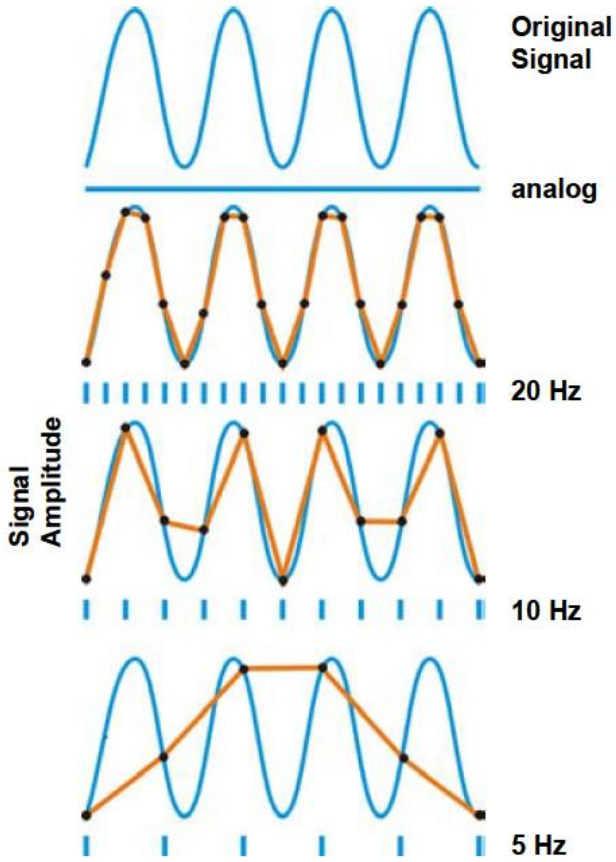

Figure 2-6. Analog signal ($f \sim 5\ Hz$) sampled at different sampling rates. The Nyquist frequency is $\sim 10\ Hz$. The yellow line depicts the digitized signal [1].

- *Resolution*. This parameter is the number of discrete values that the ADC can digitize over the range of analog input values. The resolution limits the accuracy of the measurement. A higher resolution is equal to a more accurate measurement. The value of the resolution is often expressed as a number of bits. A n-bit ADC can have 2^n discrete values to accommodate the measured analog signal. For example, a $16\ bit$ ADC will be able to represent $65,536$ values, while a $12\ bit$ ADC can only produce $4{,}096$ values. For an input range of $4\ V$ ($\pm 2\ V$), a $16\ bit$ ADC can resolve differences as small as $61\ \mu V$, while a $12\ bit$ DAQ can resolve only $976\ \mu V$ differences [15]. Because the ADC has a discrete number of values to represent a continuous signal, if the n-bit value of the ADC is too low, a quantization error can occur. This error can be reduced by increasing the n-bit value of the ADC. A 12-bit ADC is sufficient for most biomechanical studies [1].

2.3.4 Noise

Noise is described as an "irregular or random fluctuations that accompany a transmitted electrical signal but are not part of it or tend to obscure it"[5]. In other words, any signal measured that is not of interest can be considered as noise. Some noise sources come from man-made sources such as: power lines, cell phones, fluorescent lights, or other electronic circuits. These interferences can be minimized or completely eliminated.

On the other hand; non-man made noise are random signals composed of frequencies of different amplitudes and phases [16]. Although root mean squared (RMS) noise can be quantified over a long time period, its instant values cannot be determined because of its random nature.

[5] http://www.oxforddictionaries.com/us/definition/american_english/noise

Unlike man-made noise sources, there exist noises that cannot be completely eliminated, they can only be diminished.

2.3.4.1 Types of noise

There are several different types of noise that can be observed when using electronic circuits; shot, thermal, low frequency, burst and avalanche noise.

- *Shot noise*. Electronic devices with potential barriers such as diodes and transistors commonly present this type of noise [17]. Shot noise is the result of unavoidable random electron fluctuation through the potential barrier. Shot noise is independent of temperature and it has a uniform power density.
- *Thermal noise*. This type of noise is caused by random thermal motion or charge carriers (usually electrons), regardless of the applied voltage [17]. This type of carrier motion is similar to Brownian motion of particles, which is an "erratic random movement of microscopic particles in a fluid, as a result of continuous bombardment from molecules in the surrounding medium"[6]. Every conductor above absolute zero temperatures ($-273.15℃$) has electrons moving in a constant random manner, vibrating according to the temperature. Each electron possesses a charge of $1.6 * 10^{-19}C$, thus, there are small currents across the material. Although these currents averages to zero, their instantaneous fluctuations produce a voltage across the conductor. This type of noise is present in all the passive components. It is important to note that ideal pure reactive components (e.g. inductors and capacitors) do not generate thermal noise.

[6] http://www.oxforddictionaries.com/us/definition/american_english/brownian-motion?q=brownian+motion

- *Low-frequency noise*. Known as *flicker noise* because of the flicker effect that the noise generates in vacuum tubes where it was first observed. Its main characteristic is that its spectral density increases as the frequency decreases. This type of noise is present in active devices (e.g. transistors, diodes, and resistors), and even in membrane potentials in biological systems
- *Burst noise*. Consists of sudden step-like transitions between two or more levels (non-Gaussian). It can be several microvolts in amplitude, it is random and unpredictable at times. It is associated with imperfections in semiconductors, and can be minimized with optimal component selection. It is also known as *popcorn noise* because of the sound in produces when played through a speaker [18].
- *Avalanche noise*. This type of noise occurs in positive-negative (pn*)* junctions that are operated in reverse breakdown mode; it is typically associated with the Zener diodes. When the junctions of the depletion region are reverse biased with a strong electric field, the electrons acquire enough kinetic energy to collide with the atoms of the crystal lattices; these collisions create an additional electron-hole. These collisions are purely random and create pulses similar to shot noise, but larger [14].

According to the Surface ElectroMyoGraphy for the Non-Invasive Assessment of Muscles project (SENIAM[7]), the frequencies of interest in the EMG range from 10 to 500 Hz; since this is where most of the signal power is. It is important to note that in these frequency ranges, a combination of the noise types described can affect the signal of interest. Thus, the component selection and filters designed for an EMG system have to take these factors into consideration.

[7] http://seniam.org/

2.4 EMG systems

Bipolar EMG systems that use IA are the standard method to detect muscle activity. These systems are used regardless of the muscles being examined. However, there exist different muscle types with different characteristics that have to be taken into account when doing this type of measurements.

2.4.1 Bipolar

The theory for the EMG measurement with bipolar IAs is based on the structure of fusiform muscles. We will describe the differences between fusiform and penniform muscles, and in the process demonstrate why the bipolar methodology might not be the most appropriate for measuring muscle activity on other muscle architectures (i.e. penniform muscles).

2.4.1.1 Fusiform muscles

Fusiform muscles are defined as muscles that have their fibers parallel to the force-generating axis [19]. If the electrodes of the IA amplifier are aligned with the muscle fibers the propagating MUAP is measured. If we calculate the width of a MUAP with a duration of 10 ms and a conduction velocity of 5 mm/ms [20], the MUAP has a width of 5 cm. Considering the 2 cm interelectrode distance used in most studies, one can assume that the differential of the MUAP is being measured. The fiber alignment of a fusiform muscle (e.g. biceps) can be seen with ultrasound (Figure 2-7).

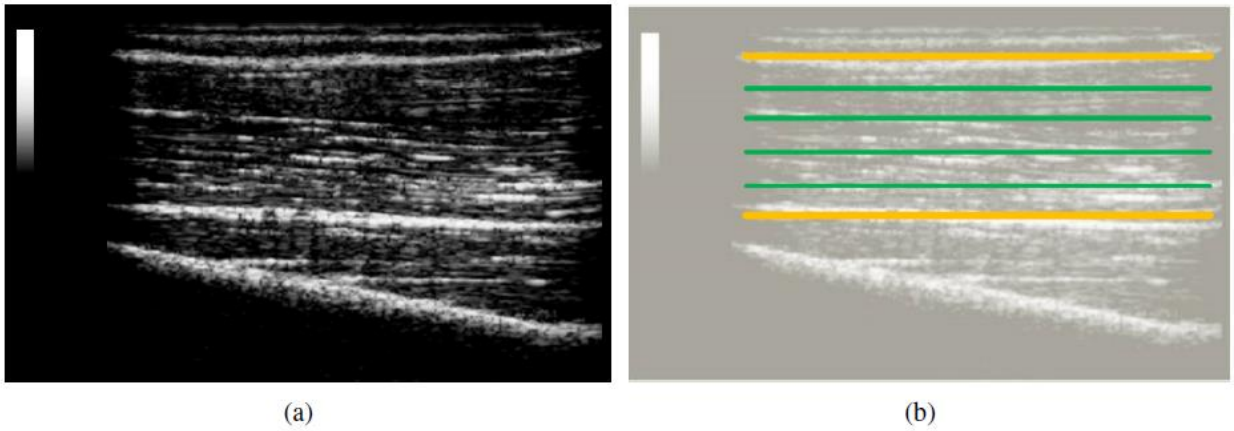

Figure 2-7. (a) Ultrasound picture of the biceps brachi muscle. (b) Same picture with the muscle fibers highlighted in green and the aponeurosis in orange [5].

However, because both of the electrodes are at different potentials there are inter-electrode currents developed in the underlying tissue that cause the amplifier to record a mixture of the signal [2]. Additionally, if the electrodes are not properly aligned with the muscle fibers, some information can be lost due to the CMRR of the IA. In the worst case scenario, when the electrodes are orthogonal to the muscle fibers, the measurement could be from two different MUs'. If the MUs' are synchronized, the common signal will be attenuated by the CMRR of the IA amplifier.

2.4.1.2 Penniform muscles

The majority of skeletal muscles are penniform muscles; their name comes from the fact that the muscle fibers have a angle with respect to the central tendon [21]. Unlike fusiform muscles, penniform muscles have a certain *pennation* angle with respect to the skin (Figure 2-8). This has to be taken into consideration when measuring with a bipolar IA. A simulation study showed that the angle of the muscle fibers has an influence on the measured sEMG potentials [22].

The potential of the deeper fibers is attenuated compared to the shallow ones (i.e. the muscle fiber closer to the upper aponeurosis). The signal can be further lost if the fibers are somewhat synchronized; if the signal arrives at the same time on both electrodes of the IA, it will be lost due to CMR.

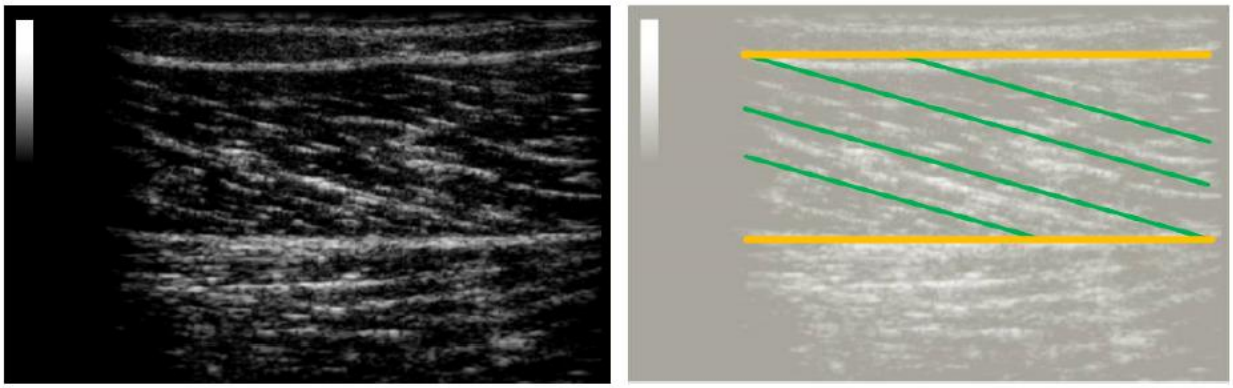

Figure 2-8. Ultrasound picture of the gastrocnemius medialis muscle. (b) Same image with the muscle fibers highlighted in green and the aponeurosis in orange. Note the pennation angle of the fibers with respect to the aponeurosis [5].

2.4.2 Monopolar

Monopolar measurements can be performed either with a voltage amplifier or with a TIA. Both of these amplifiers lack CMR, because the subtraction of the measured signal and the constant ground reference does not cancel the common mode signal (noise). With the use of a TIA to obtain EMG signals from the body we remove or inject charges at the skin surface in order to keep the potential at the electrode the same as the potential of the ground electrode. This effect is called active grounding and is achieved though the feedback loop of the TIA. This methodology has been

implemented recently to investigate the role of inter-muscular coherence in the *vastii* muscles [2]. Previous research has stated that the physiology behind the EMG signal generation is not affected by the use of the TIA [2]. This configuration has the advantage of not loosing information due to the placement of the electrodes on penniform muscles, nor to the inter-electrode currents; it was also shown that the information measured from both conventional IAs and TIAs is the same for fusiform muscles [5].

2.5 Coherence analysis

Coherence is a measure of the degree of relationship as a function of frequency between two time-varying signals [23]. It is usually presented as magnitude squared coherence (MSC), a real-valued function defined as:

$$C_{xy}(f) = \frac{\left|G_{xy}(f)\right|^2}{G_{xx} * G_{yy}} \tag{2.9}$$

Where C_{xy} is the coherence estimated for the frequency f; G_{xx} and G_{yy} are the auto-correlation spectra of the time-varying signals x and y, respectively; and G_{xy} is the cross-correlation spectra of x and y.

The method consists of obtaining two finite-time series partitioned into n segments, sampled at equally spaced data points. The samples may be overlapped or not. The fast Fourier transform (FFT) is applied to the segments that are used to estimate the auto and cross-spectral densities. The spectral densities are used to calculate the MSC estimate as shown in equation 2.9. An important advantage of this calculation is that short time shifts of the signals do not influence the coherence spectra (Figure 2-9).

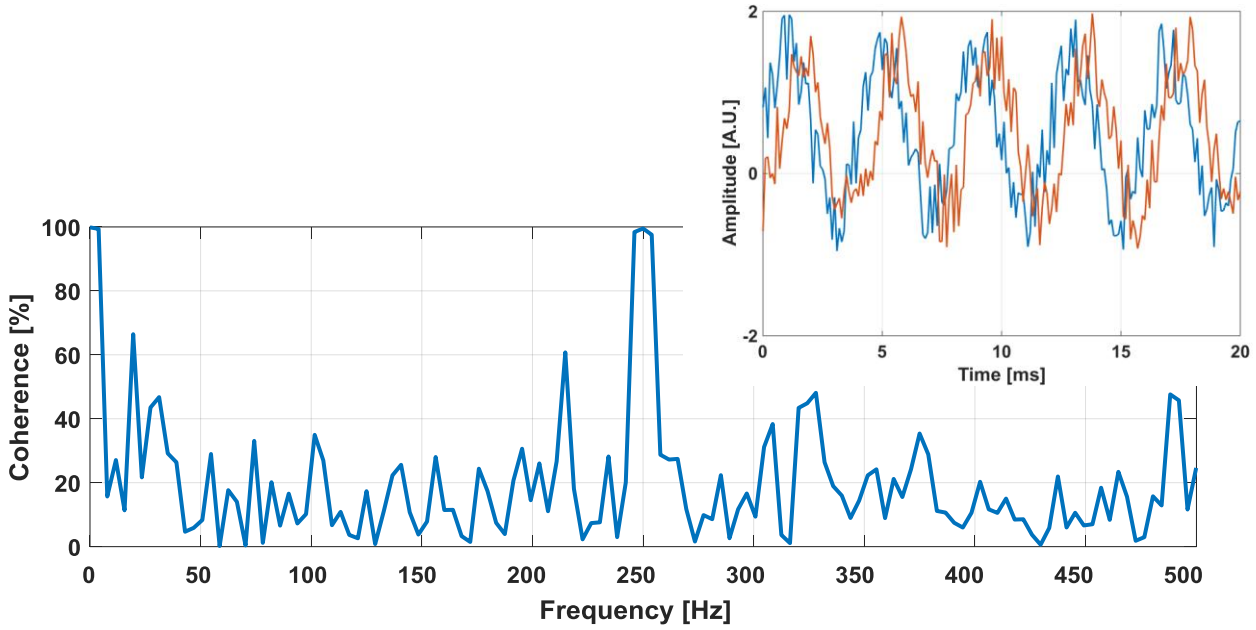

Figure 2-9. Coherence between two sinusoidal signals sampled for 1 second each at 1 kHz (top right corner). (a) two sinusoids with a frequency of 250 Hz. One of the signals lags the other in phase by π/3 radians for both signals. Embedded is white Gaussian noise of unit variance.

The literature shows that EMG coherence analysis is not a common methodology. There has been some research applied to EMG signals of single MUs [24], [25], processed data like EMG power or rectified EMG signals [26]. Recently, coherence analysis was used to assess the task dependant effect during squats [4].

2.5.1 Fatigue and EMG

Fatigue may be defined as a failure to maintain a required or expected power output [27]. The traditional experiments to investigate muscle fatigue are performed during isometric contractions (i.e. muscle contraction in which the length of the muscle does not change). However,

fatigue, on habitual conditions, is the result of a repetitive movement or exercise (e.g. performing a sport).

Currently, the literature shows that muscle fatigue manifests itself by a rising the mean amplitude of EMG. As fatigue develops, additional MUs are used to compensate for the reduction in force, thus the amplitude increases [28]. Fatigue also leads to a spectral shift of the power spectrum towards lower frequencies [1]. The median frequency (MDF) is the preferred parameter to describe the fatigue. The MDF is the value that divides the total power into two equal parts (Figure 2-10).

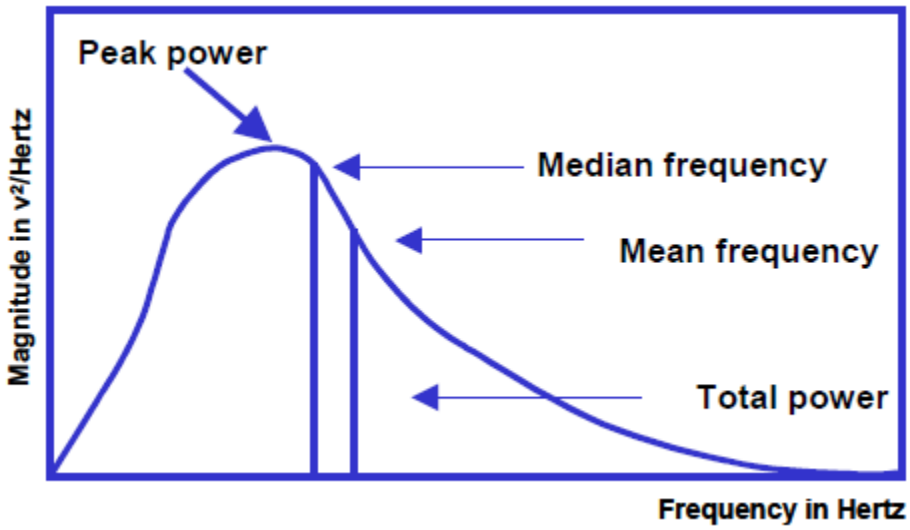

Figure 2-10. Illustration of the power spectrum of an EMG recording [1].

Recent work has also demonstrated that there exists a relation between the coherence calculation and fatigue [5]. This work shows that with several squat repetitions the coherence between the *vastus lateralis* and *vastus medialis* muscles decreases as fatigue is being achieved

(Figure 2-11). To the best of our knowledge, this is the only study that has looked at coherence as an indicator of fatigue during dynamic contractions.

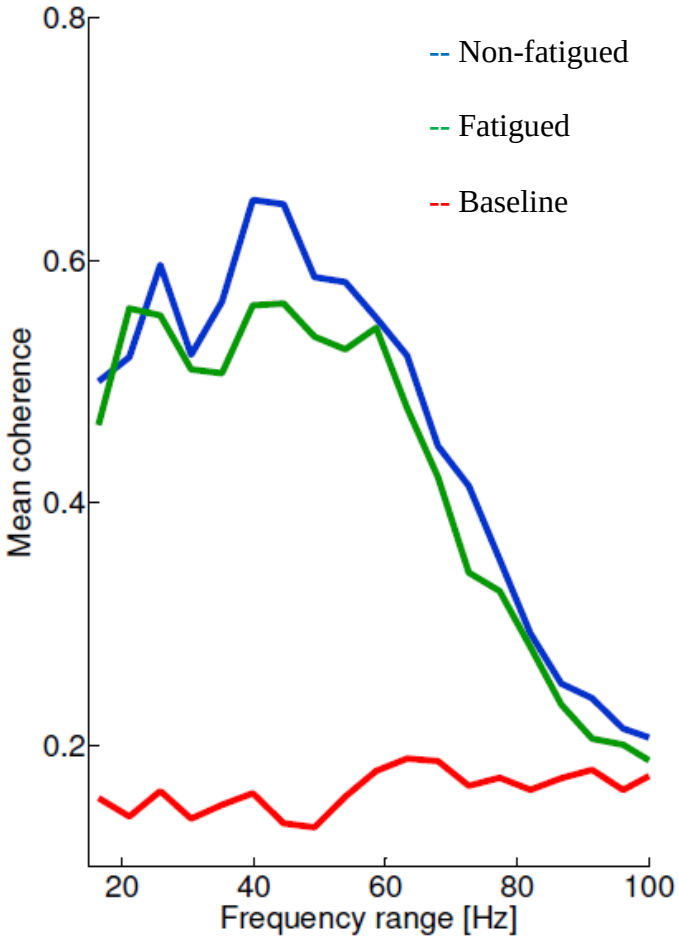

Figure 2-11. Mean coherence spectra of 18 subjects the first ten squats (blue) and the last ten squats green). The red line indicates the baseline (i.e. coherence between two random signals) [5].

2.5.2 Biofeedback and EMG

Biofeedback is defined as "A technique in which a person is taught to alter normally involuntary physiological processes, typically by using equipment to monitor associated

parameters such as blood pressure and heart rate[8]". The biofeedback technique is often used in rehabilitation and research scenarios to determine the capability of a subject to alter their normal physiological behaviour. With regards to EMG, biofeedback is commonly used to teach trauma survivors to control artificial limbs that restore the lost function [29]. Usually these techniques rely on looking at the amplitude of an acquired EMG signal from a residual limb, this information is then used to control the artificial limb. The subject receives a visual biofeedback based on the movement of the artificial limb. Through training the subject is then able to restore the lost function with the artificial limb.

Recently, there has been research that looks into the power spectra of the EMG signal to control a target on a computer screen [30] or a robotic hand for grasp [31]. EMG of a small muscle behind the ear (*auricularis superior*) was acquired and its power spectra was used to move a cursor on the screen to the desired target. Increasing the power spectra for the high frequencies ($130 - 150\ Hz$) made the cursor move in the Y direction; while, increasing the power spectra in the low frequencies ($80 - 100\ Hz$) made the cursor move in the X direction. In this study, eight subjects were trained to be able to precisely hit the indicated target (Figure 2-12). In the figure we can observe the three targets that the subjects had to hit with the cursor. The figure also shows the power differences that need to exist between the high and low frequency bands to hit each target. All the subjects were able to control the cursor and their performance was measured as the time that it took them to hit each target and return to a resting position.

[8] http://www.oxforddictionaries.com/definition/english/biofeedback

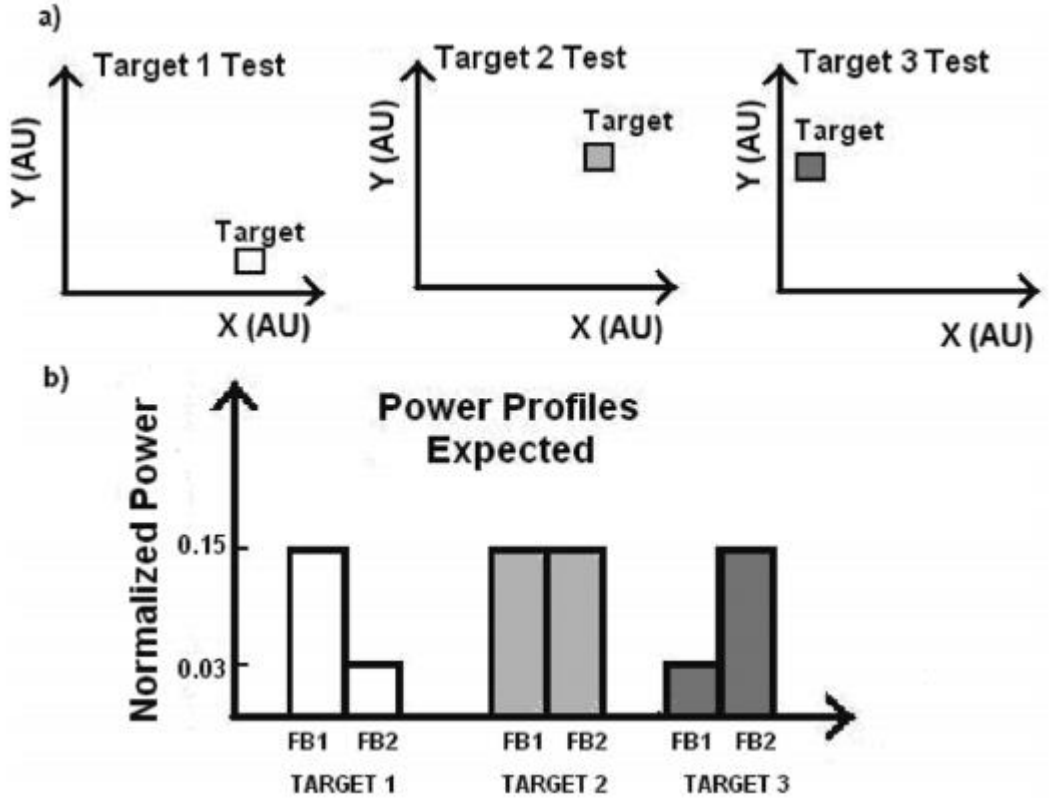

Figure 2-12. (a) Cursor-target tasks for three targets displayed to the subjects. (b) Power profiles expected for the three different target activities FB1 = 80 – 100 Hz, FB2 = 130 – 150 Hz [30].

To the best of our knowledge, these are the first studies that use two frequency bands from the power spectrum of one muscle to control a two-dimensional cursor through visual biofeedback.

As previously mentioned, EMG coherence is closely related to the power spectra. However, the literature does not demonstrate that one is able to achieve the same results using a coherence calculation approach.

2.6 Summary

This chapter discussed the basics of EMG; from the physiology to the instrumentation, and how to measure EMG activity. Different systems were described showing differences in operation, along with their strengths and limitations.

In the last section of the chapter, EMG coherence analysis was described as an indicator of fatigue, as well as its possible use for biofeedback. We now see an area of opportunity to test whether coherence can be used as an indicator for fatigue in dynamic movements as well as its implementation in a biofeedback system. Previous research suggest the use of intermuscular coherence as an indicator of fatigue during dynamic contractions [5]. However, this has only been tested for squatting movements. The inclusion of other dynamic situations can be a good indicator that intermuscular coherence is a suitable measurement for fatigue. Additionally, the use of a biofeedback system is of great interest. If it can be shown that a subject if able to voluntarily increase its intermuscular coherence, there are many possible applications for this type of biofeedback system. Both of these subjects will be addressed as part of the experimental testing of the thesis.

Chapter Three: **Hardware development**

3.1 Introduction

This chapter presents the hardware design of the proposed EMG current-amplifier, its fundamentals of operation, and a rationale of the selected components. The system consists of 4 main sections. A trans-impedance amplifier (TIA), a high-pass filter (HPF), a low-pass filter (LPF) with gain, and the isolation module. First, we will discuss about the previous work done with this type of amplifiers highlighting areas of improvement that were taken into consideration for the design goals of the proposed EMG current-amplifier.

3.2 Previous work

Previous work demonstrated that it is possible to record EMG signals with the use of a monopolar TIA instead of the conventional bipolar instrumentation amplifier (IA) [2]. Their main arguments for using the monopolar TIA over conventional bipolar IAs for EMG recordings are:

- Unavoidable inter-electrode resistances caused by bipolar electrode configuration. Since there exists an inter-electrode resistance that causes a current flow across the electrodes of the bipolar IAs. This inter-electrode resistance can cause that the electrode records similar signals to the neighboring electrodes even when the underlying signals are independent.
- The common mode rejection ratio (CMMR) of the IA eliminates, partially or completely, frequency information when recorded in penniform muscles. As mentioned in chapter two, the nature of the pennate muscles allows surface electrodes to be placed over different muscle fibers that might be innervated by distinct motor units (MUs). If the MUs recorded are synchronized in any matter, the signal generated might reach the electrodes simultaneously. The acquired signal will be degraded by the CMRR of the bipolar IA.

3.2.1 Design

For the rest of this document, the amplifier developed by von Tscharner et al. will be referred to as the *original* amplifier (Figure 3-1), whereas the newly designed amplifier will be referred to as the *new* amplifier.

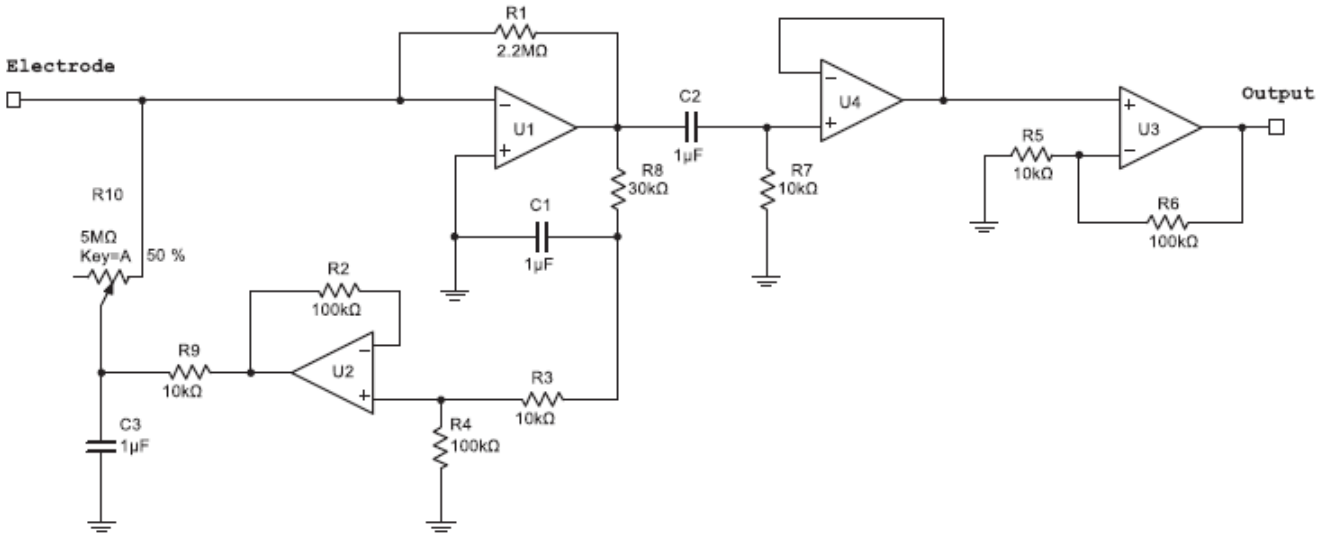

Figure 3-1. Electronic schematic of the original EMG current-amplifier designed by von Tscharner et al. [2].

The original amplifier can be divided into 4 main sections for its functioning: first, there is the TIA (implemented with U_1 and R_1 in Figure 3-1). The TIA, also known as a current-to-voltage converter takes the current of the input electrode ($I_{electrode}$) and converts it into an amplified voltage [32]. The gain of this amplifier is determined by the TIA resistor (R_1).

It is important to note that the amplitude of the current measured by the electrode depends on the muscle being recorded; muscles with a larger cross sectional area will produce larger currents [4]. The TIA resistor can be changed to amplify to the desired output voltage.

The second section of the original amplifier is a HPF. This filter is intended to diminish the drift effects caused by the electrode-skin interaction, as well as low frequency noise (e.g. motion artifacts). It is implemented with a 1st order LPF with a cutoff frequency (f_c) of 5 Hz. The low-pass frequency content is then conditioned and converted to a current which is then subtracted from the input current.

The third section of the original amplifier includes a 1st order passive HPF with a f_c of 16 Hz. The output of this filter is then fed into a OPAMP (U_4 in Figure 3-1) in the voltage follower configuration to isolate the LPF from the next section.

The fourth section is a factor of 10 gain amplifier (implemented with U_3, R_5, and R_6 in Figure 3-1). The output of this section is then passed to the data acquisition card (DAQ) for digitalization and acquisition of the EMG signal.

3.2.2 Limitations of the original amplifier

There are two main limitations with the design of the original amplifier. The first limitation is the lack of active filters. The filters in the original amplifier are passive, in other words, they are implemented only with resistors and capacitors (Figure 3-1). The filters were designed to be of 1st order (i.e. 20dB/decade roll-off). Since the signal of interest of the EMG signal is between 10 to 500 Hz [1], a 1st order filter might not have a sufficient roll-off to isolate the frequencies of interest with the selected f_c. Additionally, the original amplifier also lacks a LPF for the frequencies above $500\ Hz$ increasing the amplifier noise.

The second limitation is crosstalk. Previous work with the original amplifier has shown that it is impossible to simultaneously record EMG signals with one data acquisition system due to inter-muscular crosstalk [5]. During this study [5], EMG signals from *vastus medialis* (VM) and *vastus lateralis* (VL) needed to be recorded simultaneously. To avoid crosstalk between the two amplifiers, EMG recording of each muscle were obtained with two separate recording systems. Each system included its own ground electrode, DAQ, and battery powered laptops. To be able to analyze the signals from both systems, a synchronization device that sent a pulse signal to both systems was developed. This setup is not ideal where one is interested in analyzing multiple muscles simultaneously, as it increments the complexity of the recording by having to synchronize several systems.

M. Nann [5] describes a possible pathway for the EMG crosstalk when recording with multiple EMG current-amplifiers (Figure 3-2). In the proposed path scenario, both systems share a common ground (ankle) and DAQ. For the modelling of the crosstalk, the muscles (VL and VM) are represented as current sources, there exist inner-body impedances ($Z_1 - Z_3$), and skin impedance in the ground electrode (Z_{skin}). For the crosstalk to occur (solid red line), the signal goes from the VL into the DAQ, and back to the body through the VM muscle. As the EMG activity increases, there is a potential building under the ground electrode; if a certain threshold is reached, the signal from VL returns to VM instead of the ankle electrode.

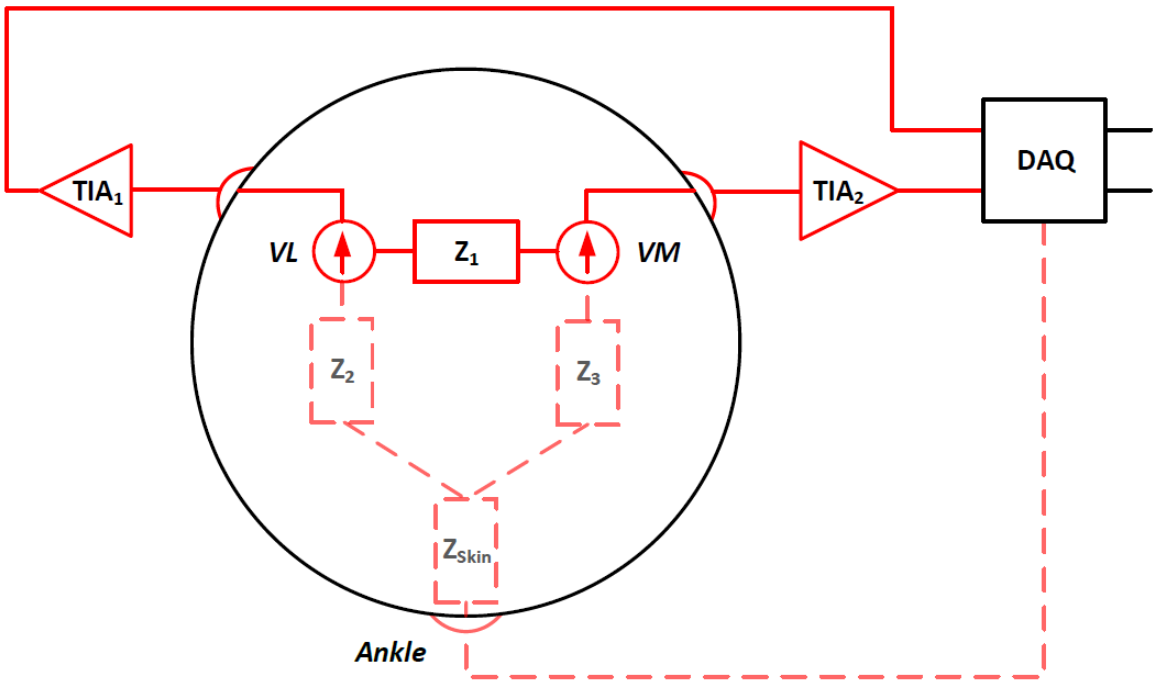

Figure 3-2. Proposed path for the original EMG amplifier crosstalk [5]. Two current amplifiers (TIA_1 and TIA_2) are connected to vastus lateralis (*VL*), and vastus medialis (*VM*) respectively with a shared ground. Interbody impedances are shown (Z_1, Z_2, Z_3), as well as the skin impedance (Z_{skin}) The solid red line marks the proposed path of the signal for the crosstalk; the dotted line marks the path that should be followed to avoid crosstalk.

The previously described configuration produces mixed recordings from both muscles (Figure 3-3). The signal recorded by both channels becomes inverted by the crosstalk. With increasing muscle activation, the inverted signal becomes more evident. The crosstalk is a problem because the recorded EMG signals do not reflect the actual muscle activity.

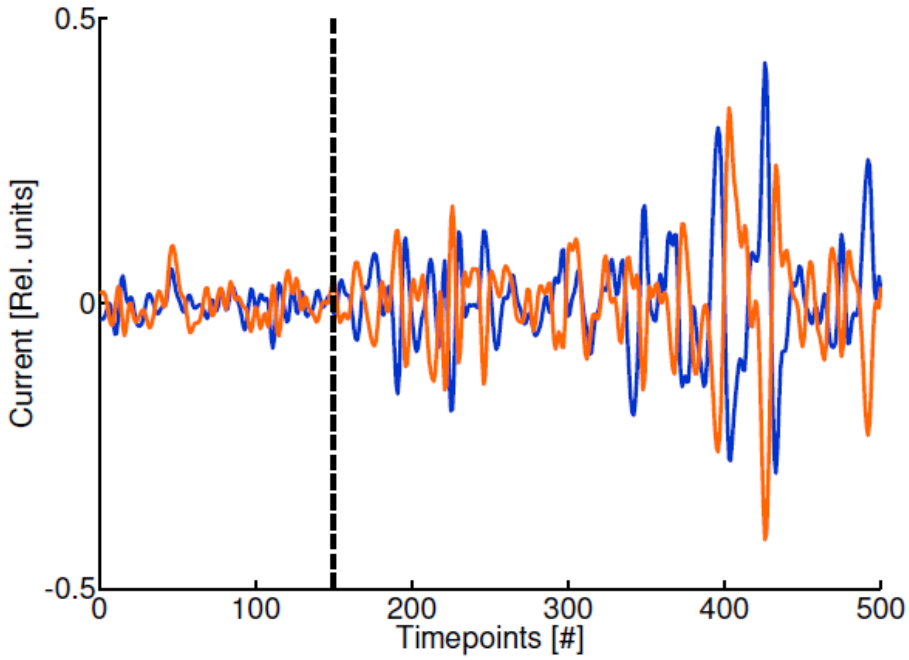

Figure 3-3. Raw EMG-currents of VL (blue) and VM (red) showing the crosstalk effect. The black line marks the downward movement of a squat. N = 1; sample rate = 2400 Hz [5]**.**

3.3 Design goals

Based on previous research [2], [4], [5], the following design goals were chosen:

- A TIA with a R_{TIA} gain selector from 100 to 500 kΩ.
- Active high and low-pass filters with a flat frequency response from 10 to 500 Hz.
- Isolation module that allows simultaneous recordings from multiple muscles.

3.4 System design

The new amplifier was designed using Multisim 14 (National Instruments™, Austin, TX, USA). The new amplifier uses the OPA140 OPAMP (Texas Instruments™, Dallas, TX, USA). This OPAMP was selected taking into account the expected EMG currents based on the original

amplifier. The expected EMG input current is $\sim 100\, nA$ (based on a measured $9\, V$ output using the schematic in Figure 3-1). The OPAMP has low noise ($151.9\, nV$ integrated noise) in the frequencies of interest ($10 - 500\, Hz$), low input bias current ($10\, pA$), and low current consumption ($1.8\, mA$). Figure 3-4 shows the block diagram of the complete EMG system.

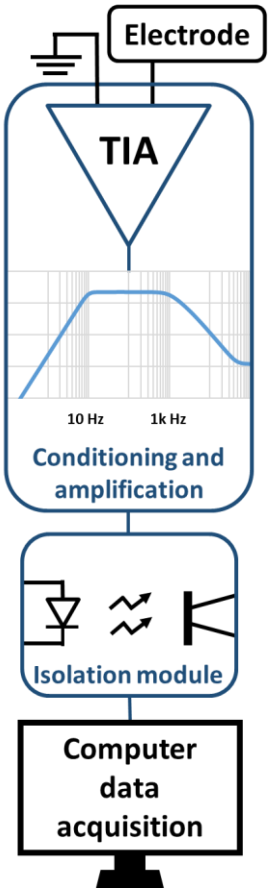

Ag/ Ag-Cl surface EMG electrodes	
Trans-impedance amplifier, (current-to-voltage converter)	
Butterworth 4th order HPF f_c = 10 Hz Butterworth 2nd order LPF f_c = 1 kHz	
Optical coupling isolation device Allows to record simultaneously from multiple muscles	
12-bit DAQ and acquisition software developed with Matlab®	

Figure 3-4. Block diagram of the new current-amplifier system with detailed design goals.

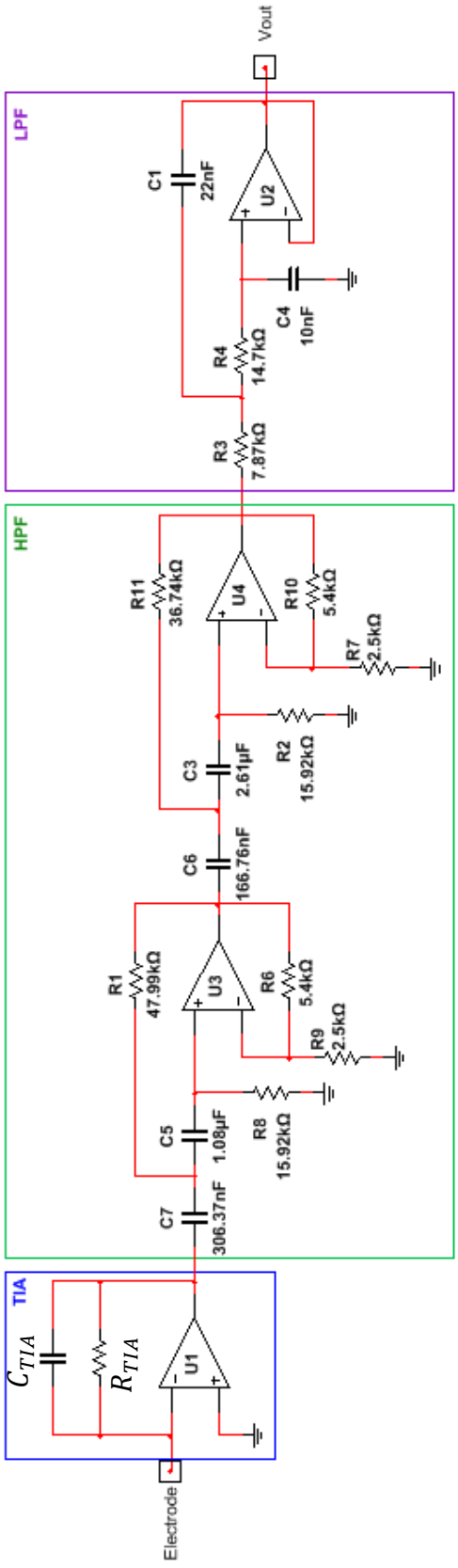

Figure 3-5. Electronic schematic of the new current-amplifier circuit.

3.4.1 Trans-impedance amplifier

The first stage of the new EMG amplifier is the TIA, which receives the input current from the surface EMG electrode and converts it into a voltage to be further filtered and amplified (Figure 3-5). The TIA has a switch to select from three different resistors and capacitors configurations for C_{TIA} and R_{TIA} (Table 3-1). The magnitude of the simulated frequency response of the three different configurations was calculated (Figure 3-6); all the configurations have a $f_c = 3\ kHz$. This f_c was chosen to leave the frequencies of interest unaltered.

Table 3-1. Resistor and capacitor values for the amplification switch of the TIA

Amplification	R_{TIA}	C_{TIA}
Low	$100\ k\Omega$	$500\ pF$
Medium	$250\ k\Omega$	$200\ p$F
High	$500\ k\Omega$	$100\ pF$

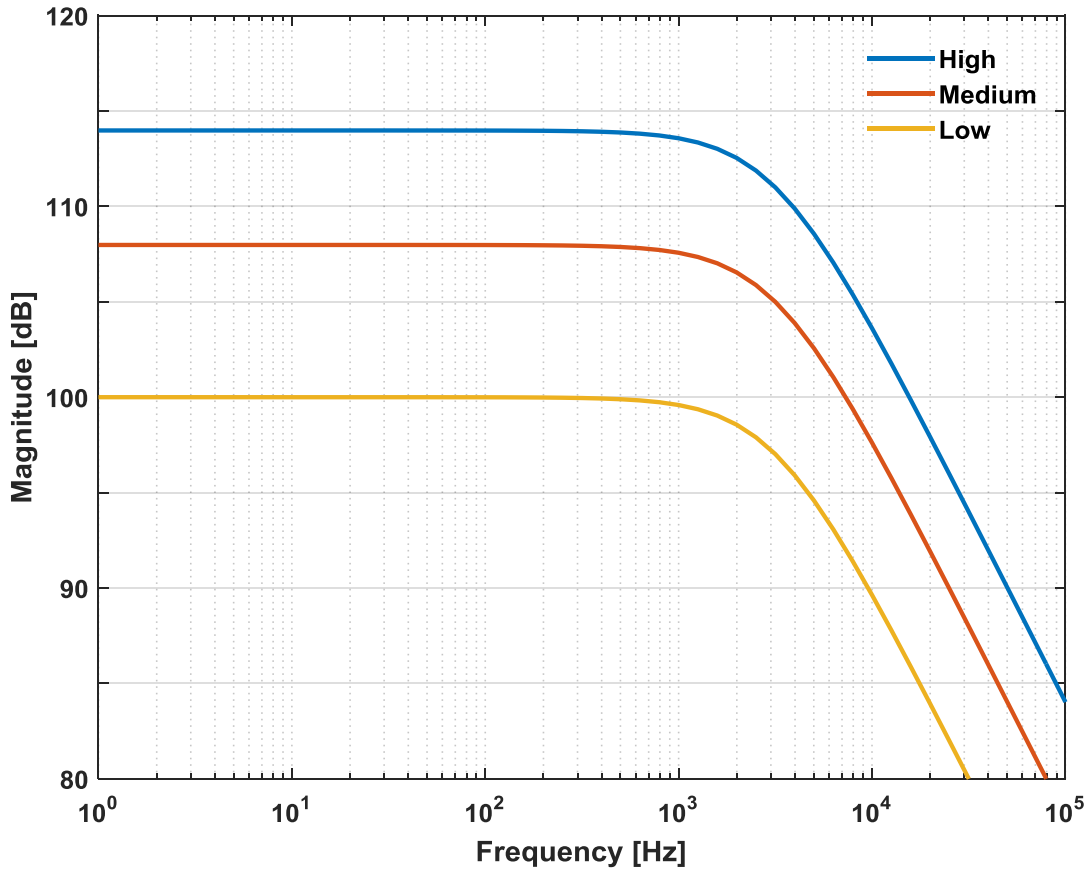

Figure 3-6. Simulated frequency response magnitude of the three gain configurations of the TIA.

3.4.2 Filtering and amplification

As previously mentioned the frequencies of interest of the EMG signal are between 10 and 500 Hz [1]. The new amplifier has two filtering stages (Figure 3-5); both filters were designed with a Butterworth response and implemented with a Sallen Key topology. The Butterworth response filters were selected due to their maximally flat magnitude (i.e. it has no ripples) in the pass band region or in the stop band [32].

The first stage of the filtering is a fourth order HPF with a f_c of 10 Hz and a gain with a factor of 10. The order of the filter was chosen to reduce the drift caused by the electrode-skin interaction.

The second stage of the filtering is a second order LPF with unity gain. This filter was chosen with a f_c of 1 kHz. This frequency was selected to obtain a flat gain response between 10 and 500 Hz.

3.4.3 Isolation

As discussed in the previous work section of this chapter, the original amplifier was unable to simultaneously record signals from multiple muscles due to a crosstalk issue. The previous solution to this problem needed a complete recording system for each amplifier (i.e. power supply, DAQ, laptop) [5].

To simplify the setup with the new amplifier, an isolation module was developed. This module allows for the simultaneous recording of different muscles with only one DAQ and one laptop. This module works with an optical coupling integrated circuit (IC). The IC selected was the HCNR 200 by Avago technologies™, the OPAMP to drive the optocouplers is the same as the one found in the new amplifier (OPA140). This IC was chosen due to its low non-linearity (0.01%) and bandwidth ($> 1\ MHz$). The optocouplers prevents crosstalk by allowing to have separate power supplies and grounds for each amplifier (Figure 3-7).

This module consists of an isolation input for each channel and a common isolation output. Each channel (marked in blue and green in Figure 3-7) has a separate power supply and ground. Since the output signal of the new amplifier is an oscillating signal around 0 V, two optocouplers are required; channel one uses one optocouplers for the positive (O2), and one for the negative

side (O4). Channel two also requires an optocouplers for the positive (O3), and the negative side (O1). This configuration does not require a baseline shift. The isolation module was designed to have a unity gain. The resistors were calculated with the equations 3.2, and 3.3 [33]. Where $K3 = 1$ and $K1 = 0.5$ from the HCNR 200 datasheet. Rf was increased from the original calculated value (with equation 3.3) from $100\ \Omega$ to $1\ k\Omega$ to limit the biofeedback resistor current (I_{Rf}) to protect the OPAMP which has a maximum output current of $36\ mA$.

$$\frac{V_{out}}{V_{in}} = \frac{K3 * RO}{Rin} \tag{3.2}$$

$$Rf = \frac{V_{in}}{K1 * I_{Rf}} \tag{3.3}$$

The current isolation module only allows two input channels; however, this can be increased as required. On the output side of the isolation there is one IC (U3) that combines the input channels. The output of the previously mentioned IC (U3), is connected to the analog inputs of the DAQ for simultaneous recording of the multiple EMG amplifiers.

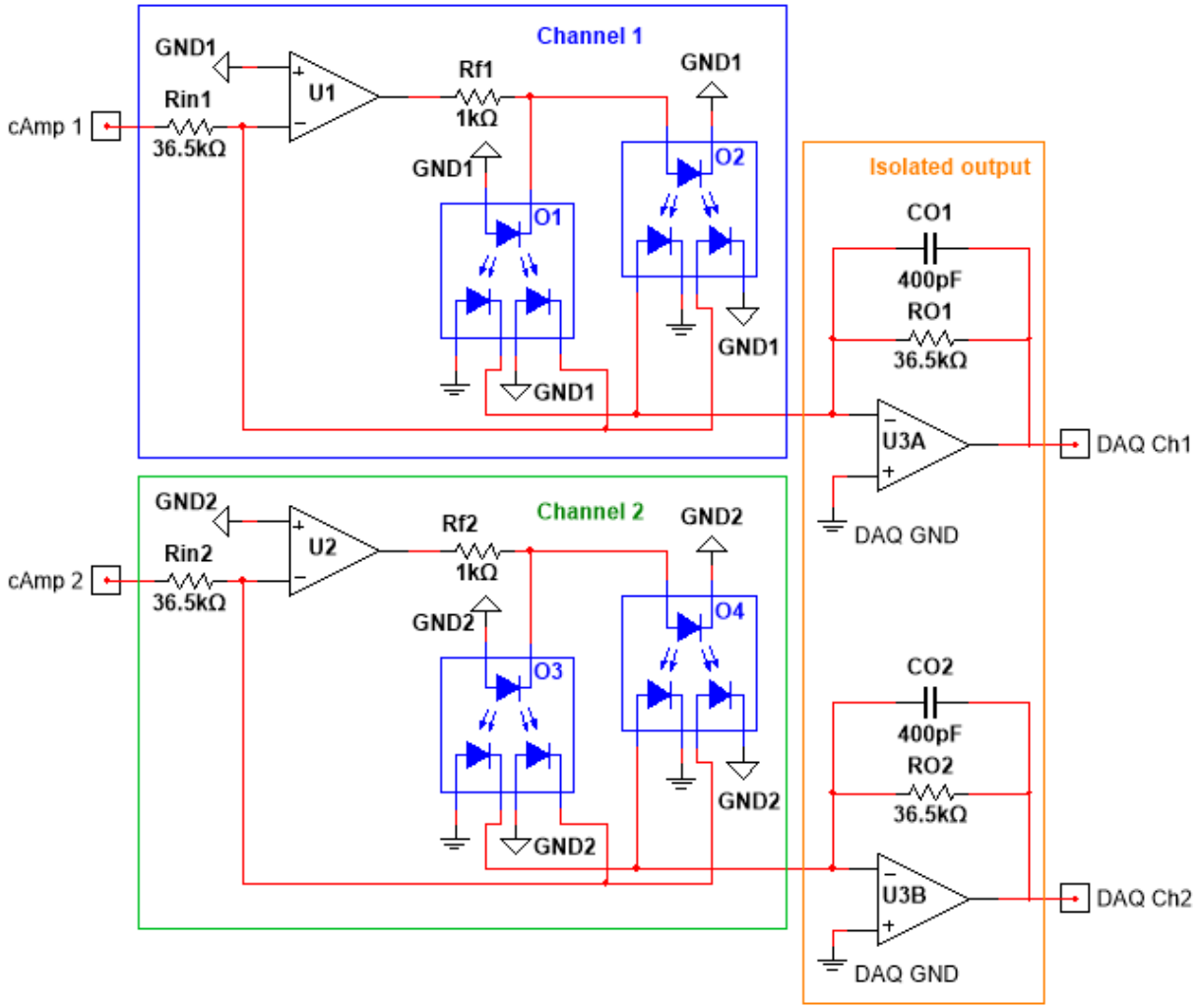

Figure 3-7. Electronic schematic of the isolation module for two new current amplifiers.

3.4.4 Simulations

Before implementing the new current amplifier in a breadboard for testing, simulations of the frequency response of the original and new amplifier were performed using the same design software (Figure 3-8). The highest gain was chosen for the new amplifier simulation (Table 3-1). The new amplifier has a lower amplification than the original amplifier because, for the purpose of this project the muscles of interest are larger (i.e. *vastus medialis* and *vastus lateralis*) than the ones that the original amplifier was designed for (i.e. *gastrocnemius medialis*).

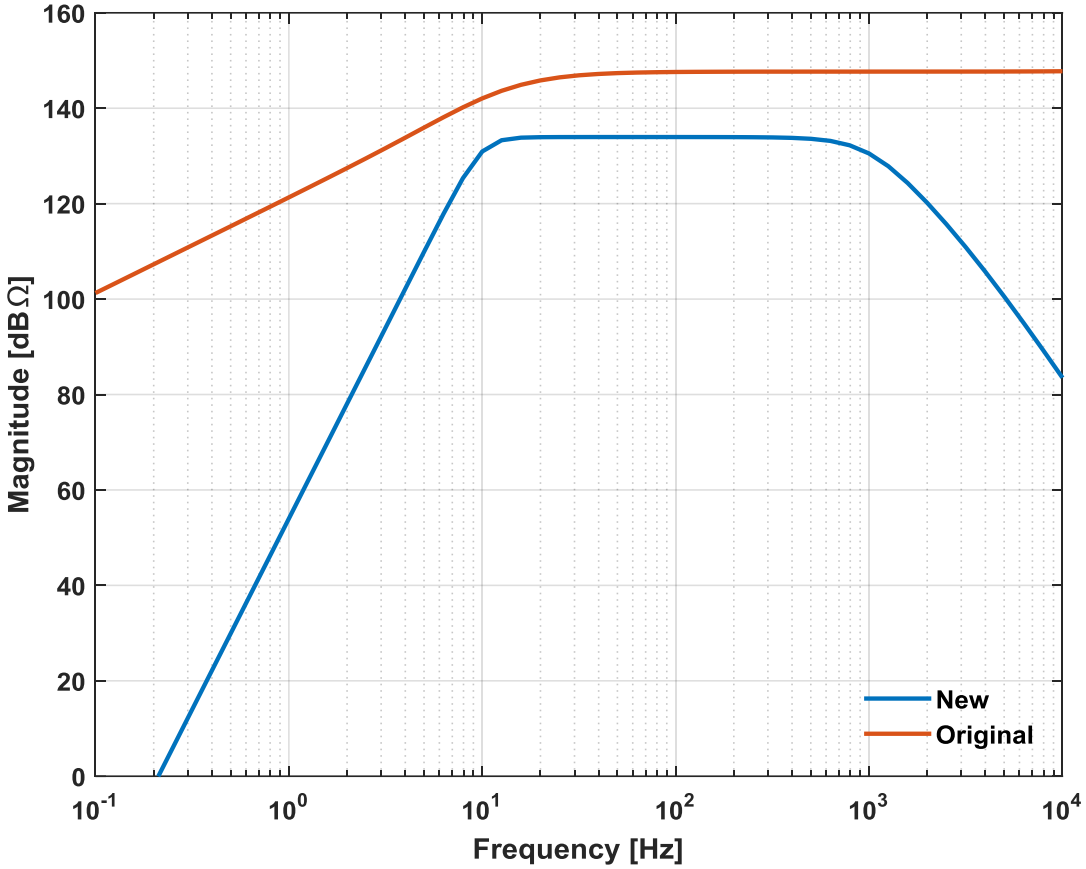

Figure 3-8. Simulated frequency response of the original and new amplifiers. Frequencies between 10 and 500 Hz are considered the frequencies of interest.

3.4.5 Characterization

Before the design and construction of the printed circuit board (PCB) the original and new amplifier were built on prototype boards to compare their performance and to verify that the new amplifier would meet the required specifications. In an effort to reduce the 60 Hz noise, all tests were performed in a Faraday cage built with a box wrapped with aluminium foil that was connected to the output amplifiers' ground.

3.4.5.1 Frequency response

The frequency response of both amplifiers was measured to ensure that the new amplifier has a flat amplification in the frequencies of interest. A trans-conductance amplifier (TCA) was used to convert the voltage from a function generator into a current to serve as the input of the current-amplifier. The IC for the TCA was the LM13700 from Texas Instruments ™. The frequency response magnitude of the original and the new amplifier were measured; for the new amplifier the highest gain setting ($500\ k\Omega$) was selected (Figure 3-9). The new amplifier showed a constant amplification in the frequencies of interest (10 - 500 Hz whereas the original amplifier does not. Additionally, the new amplifier better rejects the lower frequencies because of its higher order low pass filters compared to the original design. The same occurs in the higher frequencies, where the new amplifier diminished these frequencies and the original design amplifies them as the frequencies of interest.

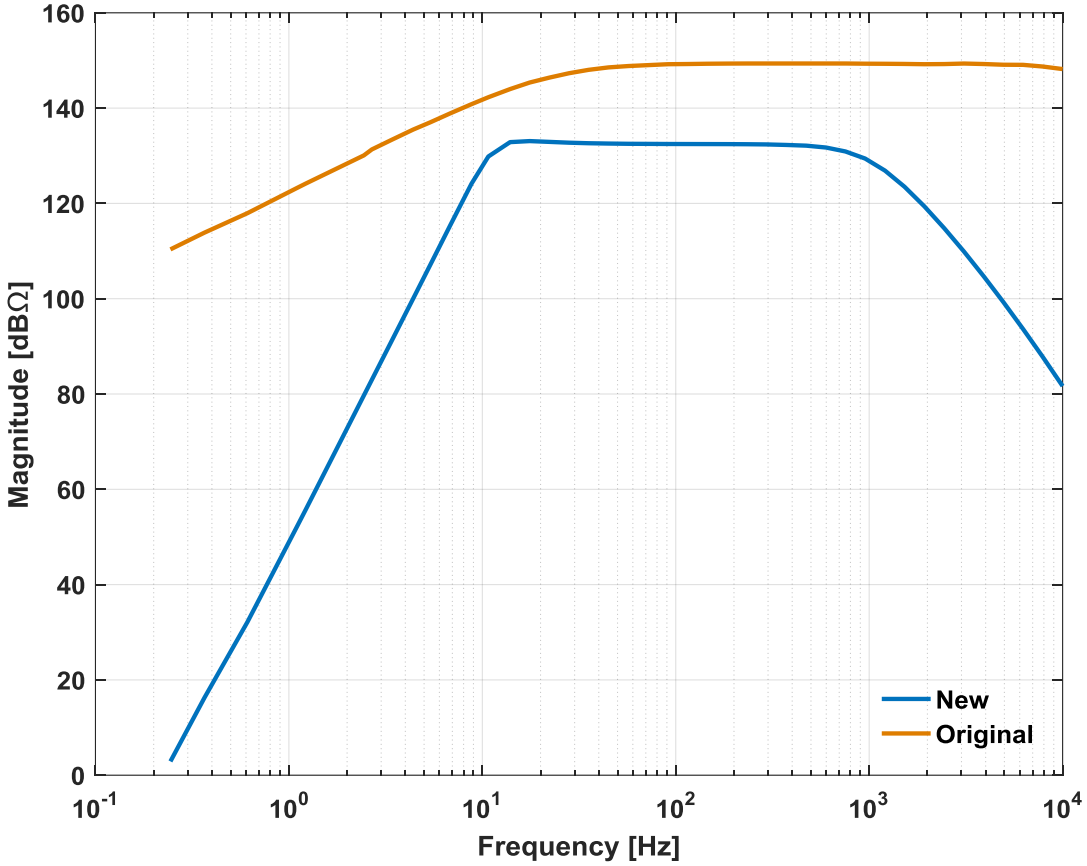

Figure 3-9. Measured frequency response of the original and new amplifiers.

3.4.5.2 Drift

The new amplifier has a steeper slope for the HPF, this is to reduce the drift of the electrode skin interaction (Figure 3-9). To demonstrate the effect of drift on the output of the amplifiers, a 15-minute recording from the right biceps muscle of one subject was acquired (Figure 3-10). For this recording the subject had his arm in the standard anatomical position (i.e. his palm facing forward with the fingers pointing to the floor). This position does not require activation of the biceps muscle, thus, only the drift will be reflected in the recording. The mean value of a 100 ms

window was calculated from the EMG data. The feedback loop of the original amplifier causes voltage fluctuations which alter the baseline of the EMG signal. This can lead to inaccurate measurements.

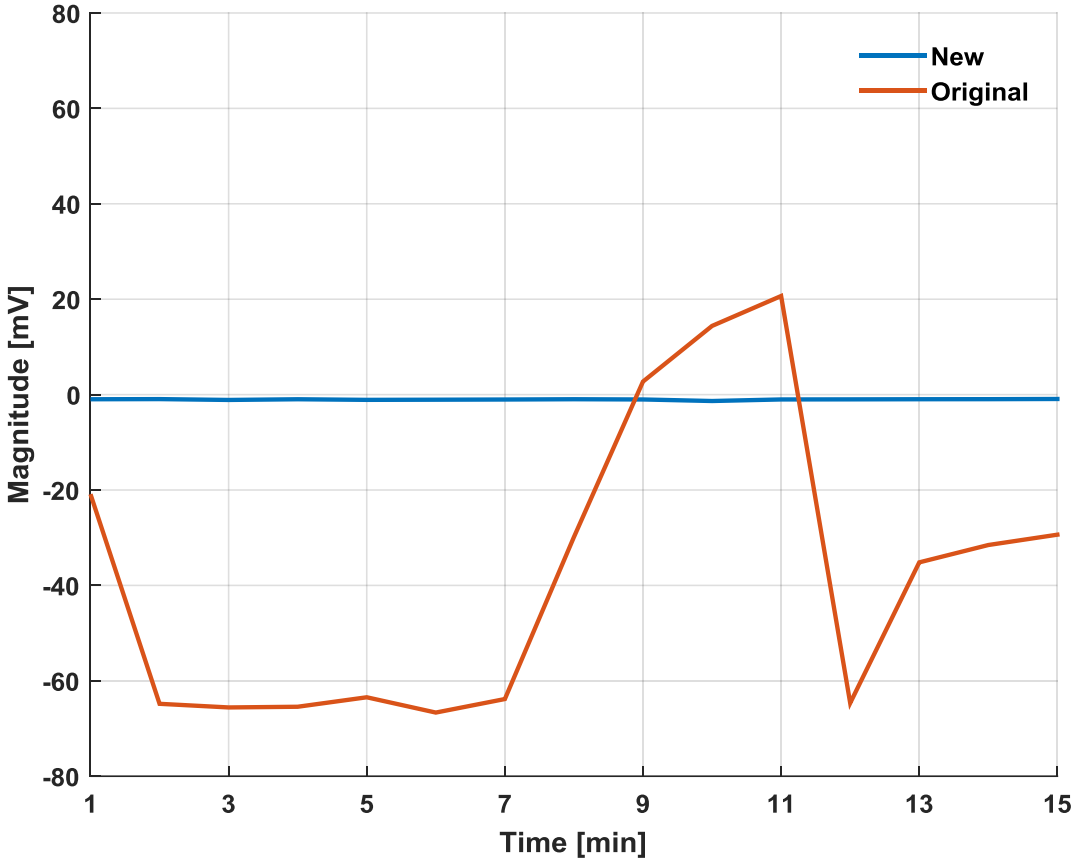

Figure 3-10. Mean output voltage calculated for a $100\,ms$ window of the original and new amplifier. Recordings are for one the biceps muscle of one subject without muscle activation.

3.4.5.3 Input referred noise

As mentioned in chapter two, there are many types of noise that can affect the measurement of the EMG signal. This electronic noise can be characterized if the output of a system is measured

when there is no input to the system. In the case of a TIA, if the input is open, the measured output will be the total noise of the amplifier. To calculate the noise that exists in each amplifier, the input referred noise spectral density was calculated. For this measurement the output of both amplifiers was measured with a spectrum analyzer (SR760, Stanford Research Systems, California, U.S.A.). The spectrum analyzer calculates the power spectrum of the measured signal. Each amplifier was placed in a Faraday cage and supplied with batteries to avoid introducing noise from a benchtop power supply. Since both amplifiers have different amplification levels, the input referred noise was calculated by dividing the measured noise by the measured amplification of each amplifier. The amplification factor was measured by using a resistor of a known value and measuring the current that the TCA produced. The output of each amplifier was measured under the same conditions as with the resistor. The output measured by the amplifier divided by the current that the TCA provided is the actual amplification factor. Note that this factor can vary slightly from the calculated amplification in the design of the amplifiers because the resistors have a tolerance of their actual value (e.g. ±1% or ±5%).

The input referred noise was calculated (Figure 3-11). The integrated RMS noise of both amplifiers was calculated for a frequency range from 10 to 500 Hz. The noise was calculated as shown in 3.4 where; PSD is the power spectral density, and df is the frequency resolution. The integrated RMS noise from 10 to 500 Hz is 3 $pA\ RMS$, and 6 $pA\ RMS$ for the original and new amplifier respectively. Despite the noise in the frequencies of interest (10 – 500 Hz) is larger for the new amplifier; the noise from 1 to 10 kHz is smaller for the new amplifier (8.73 $pA\ RMS$), than for the original amplifier (12.7 $pA\ RMS$).

$$N_x = \sqrt{\int_{f_1}^{f_2} PSD^2 df} \tag{3.4}$$

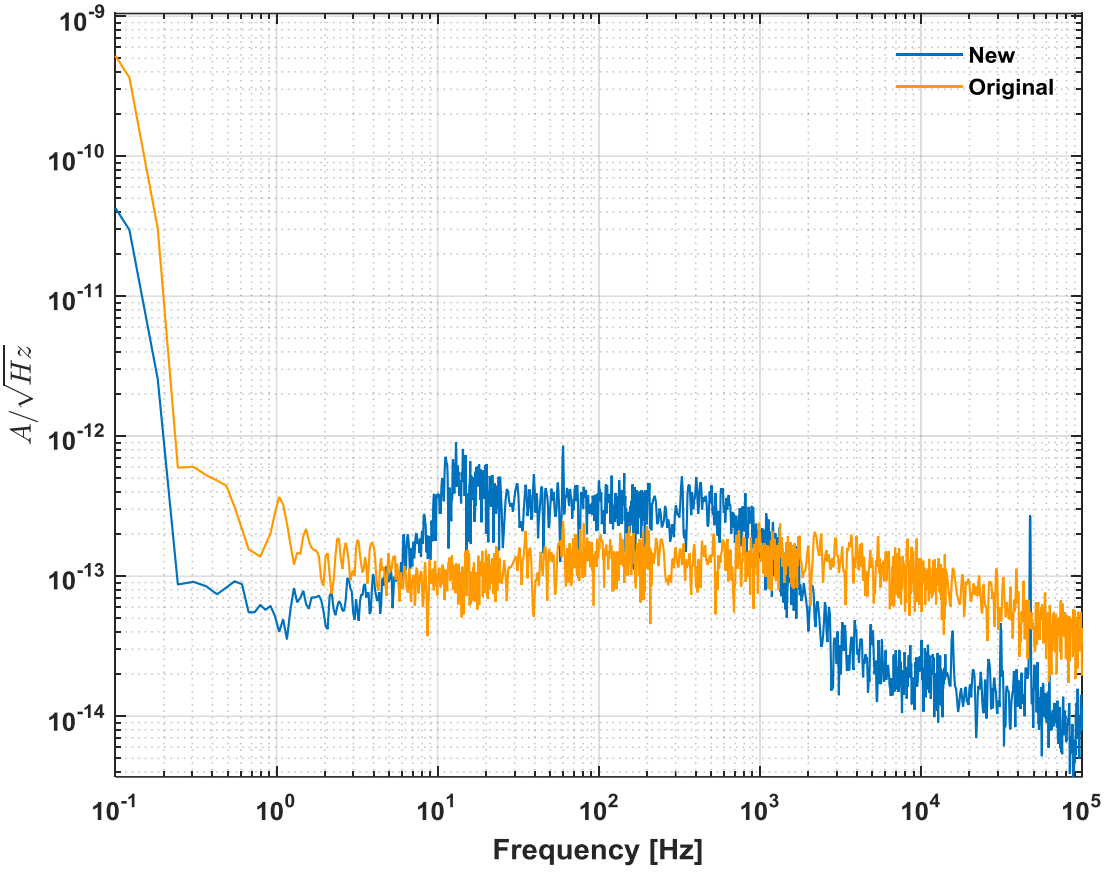

Figure 3-11. Input referred noise for the original and new amplifier.

3.4.5.4 Signal distortion

To observe any distortion that the amplifiers introduce to the input signal, the frequency spectrum of the system was obtained with the previously mentioned spectrum analyzer. A signal at $101.56\,Hz$ was used as input for the original and new amplifier. Since the amplifiers have a different gain, the input was adjusted such that the output was between $\pm 460 - 470\,mV$. Harmonic distortion can be presented as a power ratio as shown in equation 3.4

$$P_H = P_{input} - P_{harmonic} \tag{3.4}$$

The input signal to the amplifiers is generated by converting the voltage of the function generator into a current, with the TCA; as a reference for the distortion of the current-amplifiers, the distortion generated by the TCA is also measured. The measured spectrums were shifted so that the output at the input frequency was equal to $0\ dBV$. The resulting spectrum was measured for the TCA (input), the original, and the new amplifier (Figure 3-12). The input to the amplifiers has a ratio of $-52.8\ dBV$, if the amplifiers do not introduce any distortion into the signal they would show the same ratio. However, there is a distortion of $-51.4\ dBV$, and $-52.6\ dBV$ for the original and new amplifier respectively, indicating minimal additional distortion added by the amplifiers.

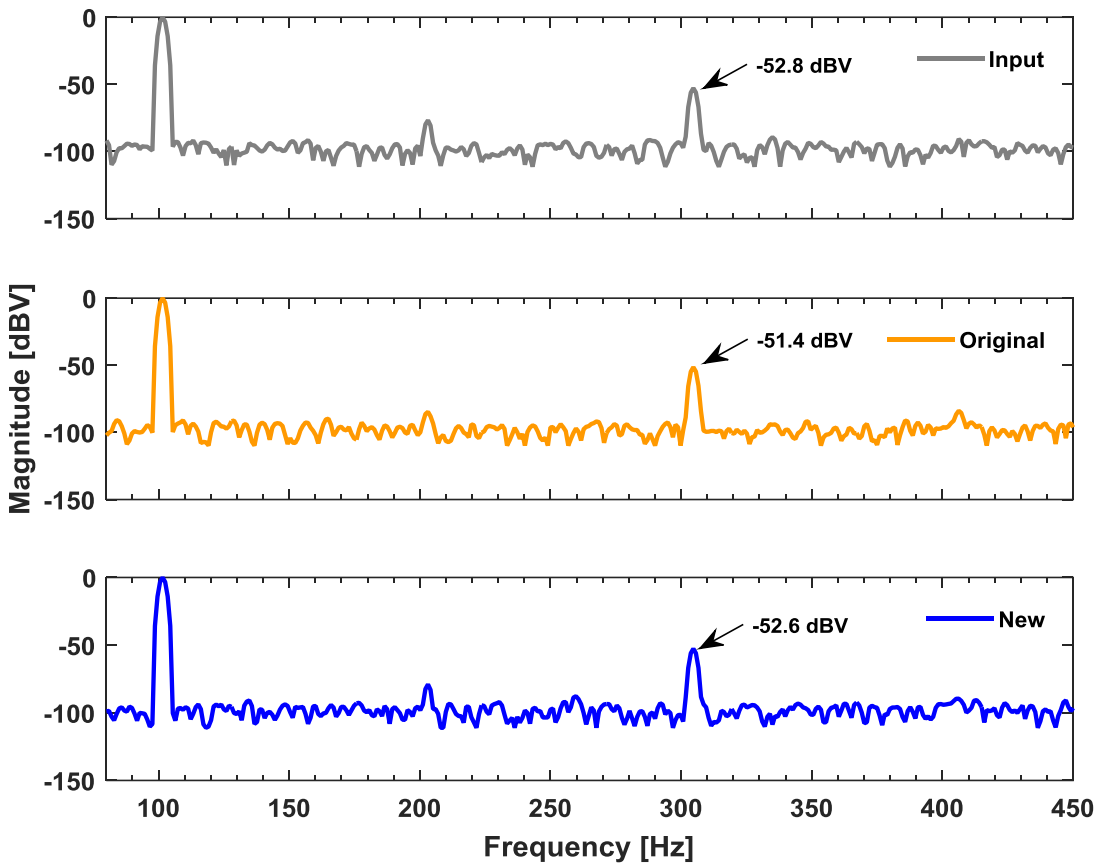

Figure 3-12. Frequency response to a 101.56 Hz input signal for the original (orange) and new (blue) amplifiers. The gray trace shows the input signal applied to both amplifiers. Marked is the magnitude of the third harmonic for each trace.

3.4.5.5 Noise reduction

Because the TIA lacks common mode rejection (CMR), other methods to reduce external common mode noise had to be taken into account. The most common type of common mode noise is the 60 Hz noise that exists in the environment. Shielded cables were used for this noise reduction in the electrode cables, as well as the connection to the isolation module. The baseline noise is

affected by the use of shielded cables in the new amplifier (Figure 3-13). These measurements were acquired from the biceps muscle of one subject without muscle activation with the new amplifier. The calculated RMS noise is $42\,mV$ for the unshielded, and $20\,mV$ for the shielded condition.

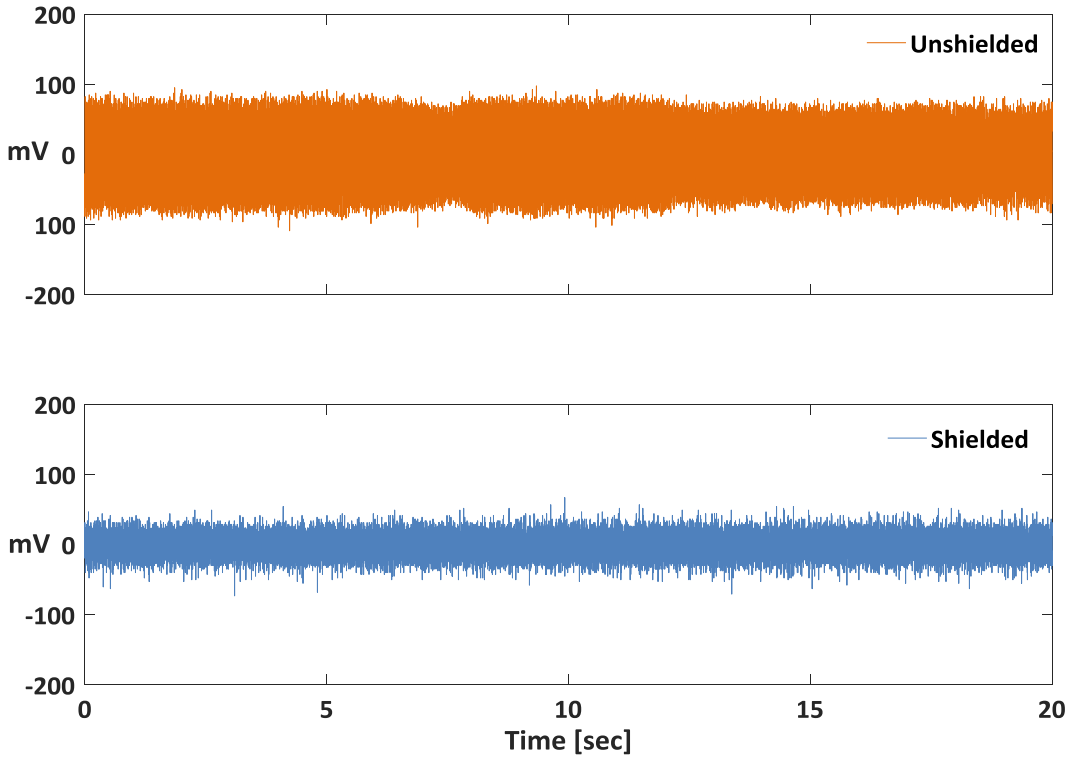

Figure 3-13. Voltage output of the new amplifier without input EMG activity with and without shielded electrode cables.

3.4.5.6 Isolation module

After testing the new amplifier, the isolation module was also tested to ensure that signals from different muscles could be obtained without the crosstalk observed in previous experiments

[5]. The isolation module was implemented on a prototype board. As previously mentioned, it is believed that the crosstalk occurs by the low impedance of the muscle electrodes compared to the ground electrodes, thus, testing for crosstalk requires measurements from a subject rather than generated signals from an instrument (e.g. signal generator). EMG activity with the original amplifier without isolation, and the new amplifier with the isolation module from the left and right biceps muscles of one subject was obtained (Figure 3-14). Ground electrodes were placed on the respective wrists. The biceps were selected because they can be controlled separately, and a visual comparison between the muscle contraction and the recorded EMG can be performed.

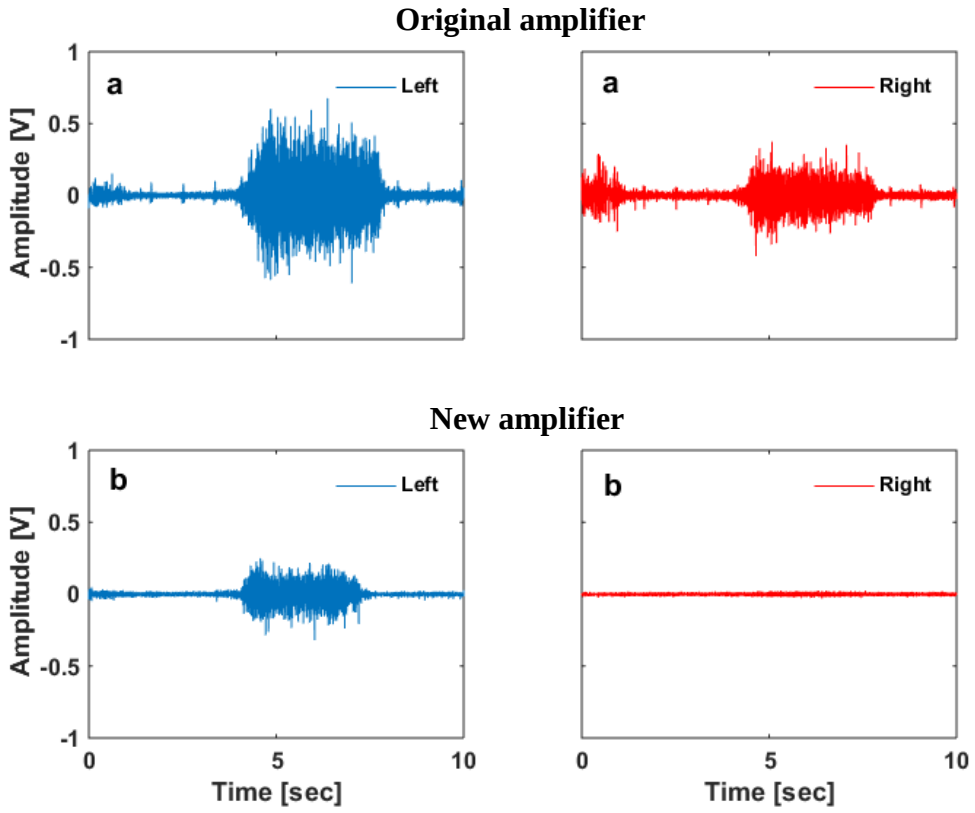

Figure 3-14. Comparison of the original (a) and the new (b) current amplifiers. A contraction of the left biceps is performed to show the functioning of the isolation module.

One subject was instructed to contract his left biceps and relax his right biceps muscle using the original amplifier without isolation (Figure 3-14.a). We expect muscle activation only on the 1st channel (blue); however, there is electrical activity in the 2nd channel (red). The same scenario was recorded with the new amplifier with the isolation module (Figure 3-14.b); in this case we only get muscle activation on the 1st channel as expected. This demonstrates that the isolation module is able to isolate the signals from different muscles when recording EMG simultaneously.

3.5 PCB development

After testing the new amplifier to characterize its response, the electronic schematics were transferred to Ultiboard 14 (National Instruments™, Austin, TX, USA)., a PCB design software. The PCB boards for the amplifier and the isolation module were designed in a dual layer board to reduce the device sizes. Although the dimension of the devices is not a critical requirement for this project, it was important to keep the new amplifier to a size similar to the original one, and the isolation module portable for an easy handling of the devices during the experiments. The resistors and capacitors chosen are the 0805 size; this allowed to have small devices without increasing the complexity of the soldering process (Figure 3-15). The isolation module was designed using the same sized components; headers were placed to interface with the batteries for supply. The amplifiers obtain their power supply from the mini USB interface with the isolation module.

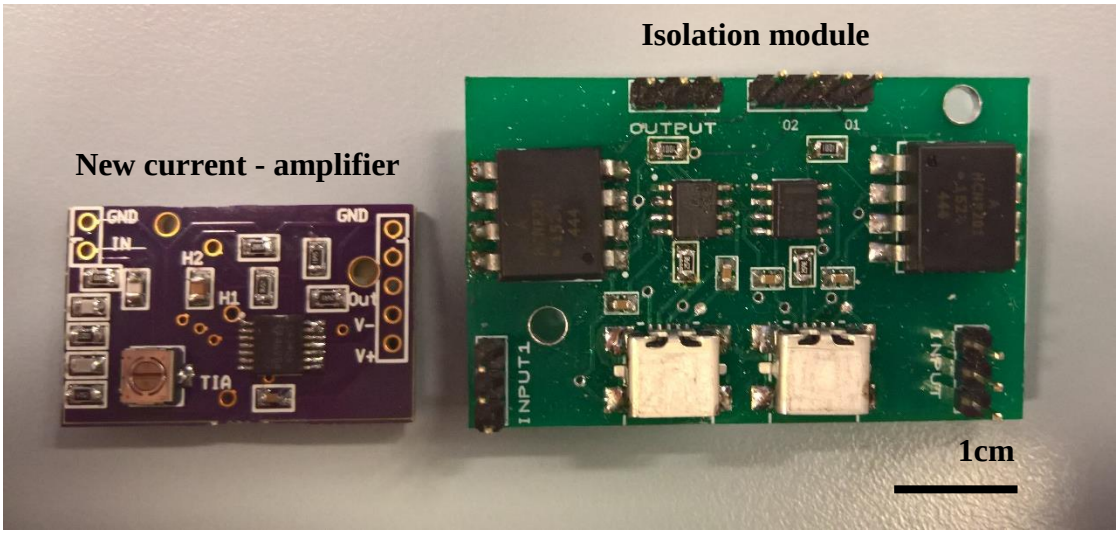

Figure 3-15. PCB of the new current-amplifier and isolation module

The electrodes and USB connectors were soldered to the PCB of the amplifier with 90° headers to avoid strain on the connectors. Since the amplifier is in direct contact with the skin of the subjects and one of the experiments will cause the subjects to sweat; a heat shrink tube was used to wrap the amplifiers. The tube has openings for the cables as well as the gain selector of the TIA.

3.6 Limitations of the new amplifier

Even though the new amplifier has a better rejection outside the frequencies of interest and drift rejection than the original amplifier, there are still some limitations when trying to use the monopolar-current amplification technique for measurement of EMG.

Compared to the IAs, the TIA lacks CMR. This fact makes the new and old amplifiers susceptible to 60 Hz noise. This type of noise is very common since its produced by the power lines of the instrumentation used in sports and medicine research (e.g. treadmills, dynamometers,

ergometers). Even with the inclusion of shielded cables the current-EMG amplifiers have noticeable 60 Hz noise, which is filtered in software using a line averaging method [2].

The second major limitation is associated with the isolation module. Although the new amplifier setup is simplified by the use of the isolation module in the sense that we only require one DAQ and one computer for acquiring data; the isolation module requires separate power supplies for each amplifier connected to the isolation module, as well as one power supply for the output side of the isolation module. This fact still complicates the setup since we need a separate ground electrode for each amplifier as well as the power supplies previously mentioned. As a reference, for the experiments detailed in the fourth and fifth chapters the new amplifier requires six 9V batteries and four EMG electrodes (two electrodes for the muscles, and two ground electrodes), whereas a conventional system would require two batteries and five electrodes (four electrodes in the muscles, one ground electrode).

Although it is not a limitation per se, the isolation module is designed to have an input range of ± 2 V due to the currents allowed by the light emitting diodes (LEDs) of the optocouplers in the input side of the isolator. If the application requires a larger input range, the resistors should be recalculated to avoid a large forward bias current that could damage LEDs.

3.7 Summary

In this chapter, we described the development of the hardware for the new EMG current-amplifier. The design of the amplifier and isolation module were described to fulfill the system requirements. Measurements were performed in the original and new amplifier to demonstrate that the new amplifier exceeds the performance of the original one. Lastly, the limitations of the new amplifier were discussed.

The instrumentation described in this chapter will be used in the next two chapters to understand the role of inter-muscular coherence during fatiguing exercises, as well as the effect of biofeedback into the coherence of the lower limb muscles.

Chapter Four: **Effect of fatigue on intermuscular coherence**

4.1 Introduction

Motor unit (MU) synchronization has been measured with monopolar needle electrodes for the vastii muscles [34]; their findings showed that MU of different muscles are synchronized (intermuscular synchronization). However, these findings were obtained during isometric contractions (i.e. contractions in which the muscle length does not change). Isometric activities do not necessarily reflect muscle activities during common movements in humans. Thus, experiments with dynamic contractions are more appropriate to understand about the behavior of the intermuscular synchronization [4].

Previous studies have demonstrated that intermuscular coherence (i.e. the similarity of frequency content in electromyography signals from two different muscles) occurs during dynamic contractions such as squat movements [4]; it was also shown that the level of coherence between the lower extremity muscles (e.g. *vastus lateralis* (VL) and *vastus medialis* (VM)) depends on the complexity of the task. Additionally, a similar study showed that coherence decreases when the muscles become fatigued during the squatting movement [5]. Muscle fatigue may be defined as the failure to produce a required or expected force output [27]. To the best of the author's knowledge the study by Nann [5], is the first study that uses intermuscular coherence to assess muscle fatigue instead of using the more conventional measures such as the decrease in the mean and/or median frequency (MDF). However, the coherence methodology to quantify muscle fatigue needs to be further tested in other dynamic situations.

The median frequency has been proposed as a method to assess muscular fatigue using frequency-domain features of the electromyography (EMG) signal [35]–[44]. MDF is the frequency at which the EMG power spectrum is divided into two regions with equal power [45].

This methodology is commonly used during static muscle contractions. During dynamic contractions its results are often contradictory [46].

The purpose of this study is (a) to calculate the coherence between the vastus medialis and vastus lateralis muscles during a cycling task to compare a fatigue with a non-fatigue condition, (b) to compare the coherence results with the median frequency method when comparing a non-fatigued with a fatigued condition.

A cycling task, in a stationary bicycle, has been chosen because it is a dynamic task that might require a lower level of coherence than the squatting movement from previous research [4], [5]. The squatting movement requires two tasks from the muscles, the lowering of the center of mass, and the stabilization of (especially the mediolateral) balance; both of these tasks require a coherent activation of the vastii muscles. On a bicycle, the coherent activation of the vastii muscles might be lower due to the fact that the movement does not require a stabilization of the center of mass or the mediolateral balance. Nevertheless, the vastii muscle must still work in synchrony to ensure optimal force to perform the pedalling motion. Thus, the effect of fatigue could be different in a cycling movement where coherence might not play an essential role.

4.1.1 Hypothesis and purpose

The hypotheses for this experiment are:

Hypothesis #1

Intermuscular coherence between VL and VM will decrease during a cycling activity when the subjects start to become fatigued.

Hypothesis #2

In a dynamic situation, such as cycling, the Median Frequency method, MDF, will not show a significant difference when comparing a non-fatigued and a fatigued condition.

4.2 Materials and methods

Seventeen healthy male subjects (25.3 ± 1.7 YO) were recruited for the experiment. This sample size was chosen based on a priori power analysis based on previous research that analyzed fatigue during squatting movements [4]. The power analysis showed a required sample size of twelve subjects. Seventeen subjects were chosen because the task for this experiment is a more constrained movement than the squatting movement. All subjects reported to do exercise on a regular basis (at least 3 hours per week), and had no lower limb injuries in the preceding 12 months.

Subjects used a stationary cycle ergometer. The seat height was adjusted to ensure that the subjects had a 30° knee angle at full leg extension based on previous literature [47], as well as to keep a consistent position of the subject in the ergometer. Surface EMG of the vastii muscles was assessed with the previously described new current-amplifier (chapter 3). The location of the *Ag-AgCl* surface EMG (sEMG) electrodes was determined by palpation of the muscles during a leg extension movement. Skin preparation included shaving of the area of interest, light skin abrasion with sanding paper, and final cleaning with isopropyl alcohol [1]. The adequate signal amplitude was verified by asking the subject to perform several contractions before the experiment. The signal amplitude was visually inspected to be at around $\pm 1\,V$ during a leg contraction; the amplification factor to ensure the output of +/- 1V was recorded for each subject. Pulmonary gas exchange (VO_2, CO_2, and RER) and heart rate were assessed with a portable COSMED K4b2 unit (COSMED Inc., California, USA).

4.2.1 Protocol

Participants completed two sessions of data collection. Sessions were at least 3 days apart from one another to ensure that the subjects performance was not compromised due to post-exercise fatigue [48].

The first session consisted of an incremental protocol. Subjects were asked to maintain 70 rpm in the cycle ergometer. Power output started at 100 W for all subjects, increments of 25 W were performed at two-minute intervals. The test was considered as terminated if any of the following conditions occurred:

- The subject could not maintain 70 rpm for a period longer than 30 seconds
- Respiratory exchange ratio (i.e. the ratio of the net carbon dioxide output to the simultaneous uptake of oxygen) was higher than 1.15 for a period of 30 seconds
- Volitional exhaustion (i.e. the point at which a person cannot perform a muscular contraction, and voluntarily terminates the contraction [44]).

Verbal encouragement was provided to the subjects in an effort to extend the protocol time, regardless of debate on the validity of this matter [48].

The test on the second session consisted of cycling at a constant power output of 85% of the highest power output reached during the first session. The highest power output was considered as the power output of the last stage in which the subject was able to endure for at least 30 seconds. Prior to the test, a 5-minute warm-up at 50% the max power output was performed followed by a 2-minute rest. The three conditions to terminate the first session applied for the second session as well.

4.2.2 Data processing

After the data was acquired, the coherence between VL and VM was computed using custom scripts and functions with Matlab 2016™ (Mathworks Inc., Natick, MA.). The processing function algorithms are detailed as follows.

4.2.2.1 Event detection algorithm

The event detection algorithm determines the data that will be used to calculate coherence. As mentioned in chapter two, the magnitude square coherence (MSC) determines the similarity in frequency content of two signals. Since the new amplifier lacks common mode rejection (CMR), noise will be present in both EMG signals. To find the times where the muscles were active, the signal was first filtered for the 60 Hz noise. The signal was filtered with a line-frequency averaging method [2]. This method allows removal of the 60 Hz noise without inducing a notch effect (i.e. it does not attenuate the frequencies close to 60 Hz) in the signal or altering its phase [2]. After the signal was filtered at 60 Hz noise, a wavelet filter was used to determine the peak of the EMG activations. The wavelet filter allows an envelope of the signal to be formed (Figure 4-1, middle graph). The local peak of the envelope was then selected as the middle of a bin of 2^{10} (1024) data points (i.e. $\sim 426\ ms$); this bin is selected as the active region of the EMG. The 2^{10} points value was chosen because it closely approaches the data points in each activation of the experiment later described without including the relaxed zone (i.e. the region without EMG activation that has the most evident 60 Hz noise). The data points selected (Figure 4-1, red trace) constitute discrete events, multiple of these events were then used for the coherence calculation.

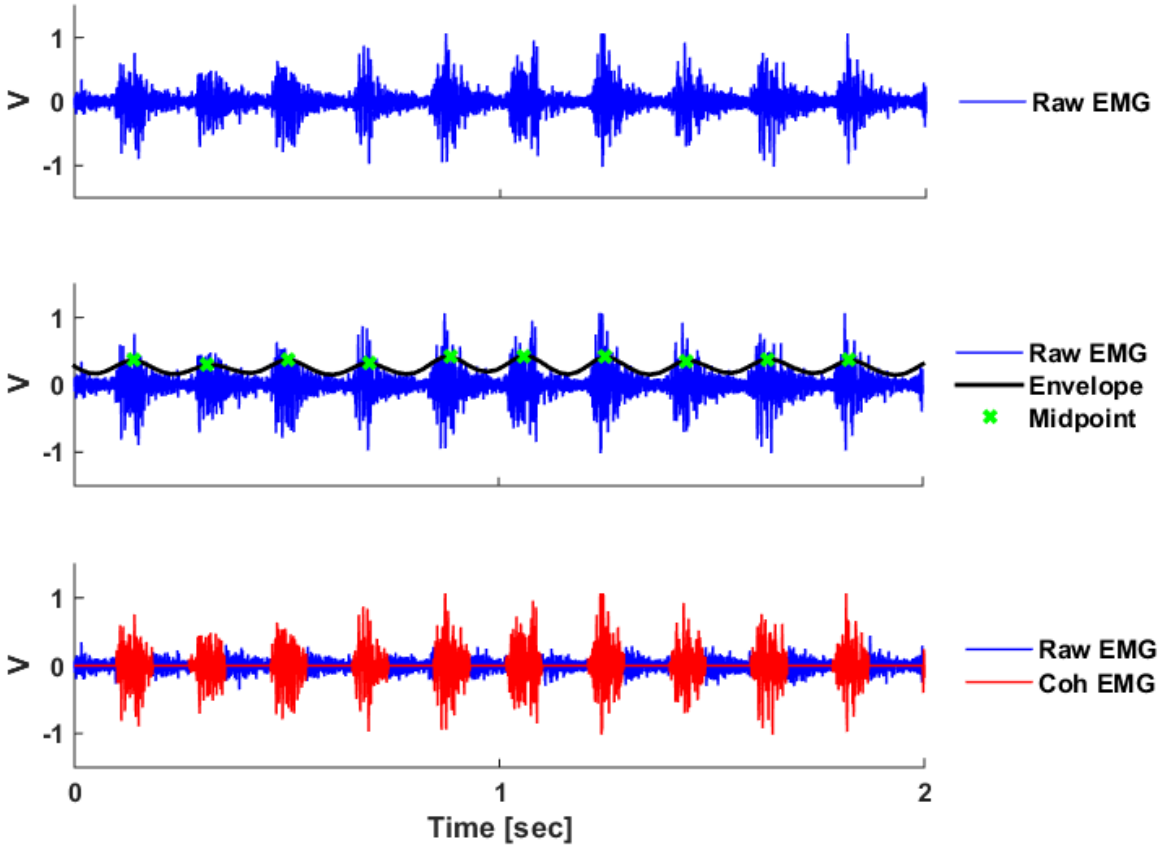

Figure 4-1. Raw EMG (top), wavelet filter envelope (middle), and EMG data used for coherence calculation (bottom). Traces show EMG data from VL from one subject during the cycling protocol. Sample rate = 2400 Hz.

4.2.2.2 Coherence analysis

Coherence analysis is a measure of the similarity between the frequency spectra of two signals. A representative coherence calculation during the cycling protocol is shown in Figure 4-2. Although the coherence calculation is independent of small time shifts, if one signal is shifted enough, both of them begin to look like incoherent signals. To determine the baseline coherence, the coherence between two non-simultaneous events was calculated.

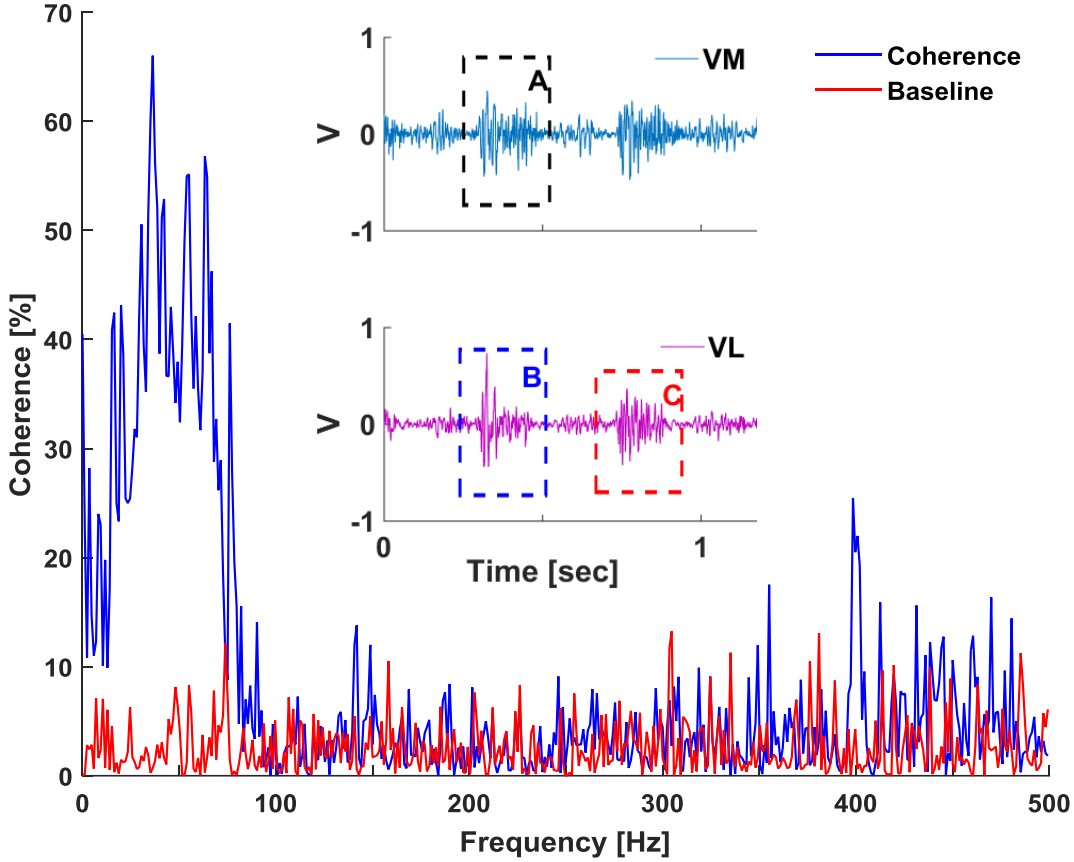

Figure 4-2. Raw coherence calculation with baseline for 20 EMG activations. N = 1. The smaller plot shows the muscle activations used for the coherence and baseline calculation. The coherence is calculated using simultaneous muscle activations (i.e. A and B). The baseline is calculated using non-simultaneous muscle activations (i.e. A and C).

The calculated coherence decreases above $100\,Hz$ to baseline levels Figure 4-2. A coherence of interest value (CoI) will be considered as the area under the curve between $10-100\,Hz$ (i.e. where the coherence is above the baseline level). Similar frequency ranges has been previously reported in the literature for intermuscular coherence measured with current-amplifiers;

15 – 100 Hz [4], < 120 Hz [2], 25 – 100 Hz [3]. The variable of interest in this study is the "normalized coherence", which is the coherence of interest shown as a percentage of a 100% coherence.

Since coherence is an estimation, it is susceptible to noise, and activation-to-activation variation. To determine an adequate amount of data required to have a stable measure for the coherence, the cumulative coherence was calculated (Figure 4-3). After 20 events the slope of the cumulative coherence changes less than 1%. Thus, twenty events were chosen for all further coherence calculations.

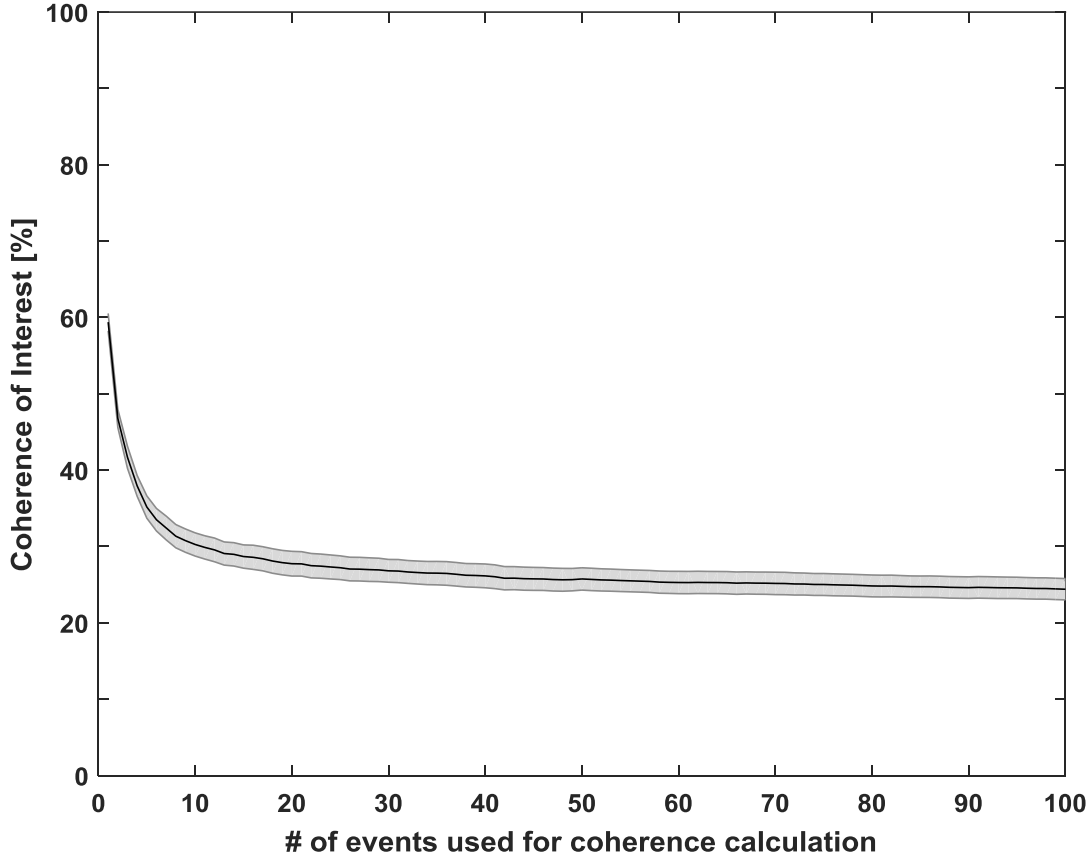

Figure 4-3. Normalized additive coherence of interest calculation. Mean ± SEM, N = 17.

Three sets of 20 EMG activations were used for the coherence of interest computation (i.e. 60 EMG activations in total); this was done for the beginning and end of the second session for each subject. The Coherence of interest, CoI, was computed to compare a non-fatigued vs a fatigue state. The median frequency (i.e. the frequency at which the power spectral density area of the EMG signal is divided into equal parts) was calculated for the same EMG data as the Coherence of Interest, CoI, for the VM and the VL. The median frequency was calculated for the frequency range from 10 to 500 Hz. Additionally, a histogram of the change in coherence of interest, CoI, was calculated (i.e. the coherence in the fatigue condition normalized to the coherence of the non-fatigue condition).

For the statistical analysis, the paired samples t-test was used to determine differences between mean of the non-fatigue and the fatigue condition for the coherence of interest and the MDF for all subjects.

4.3 Results

The results for coherence of interest are showed in Figure 4-4. For 13 subjects, the coherence of interest decreased $19.9 \pm 3.5\%$ (mean ± SEM). On the other hand, for 4 subjects increased by 7.7 ± 4.2% (mean ± SEM).

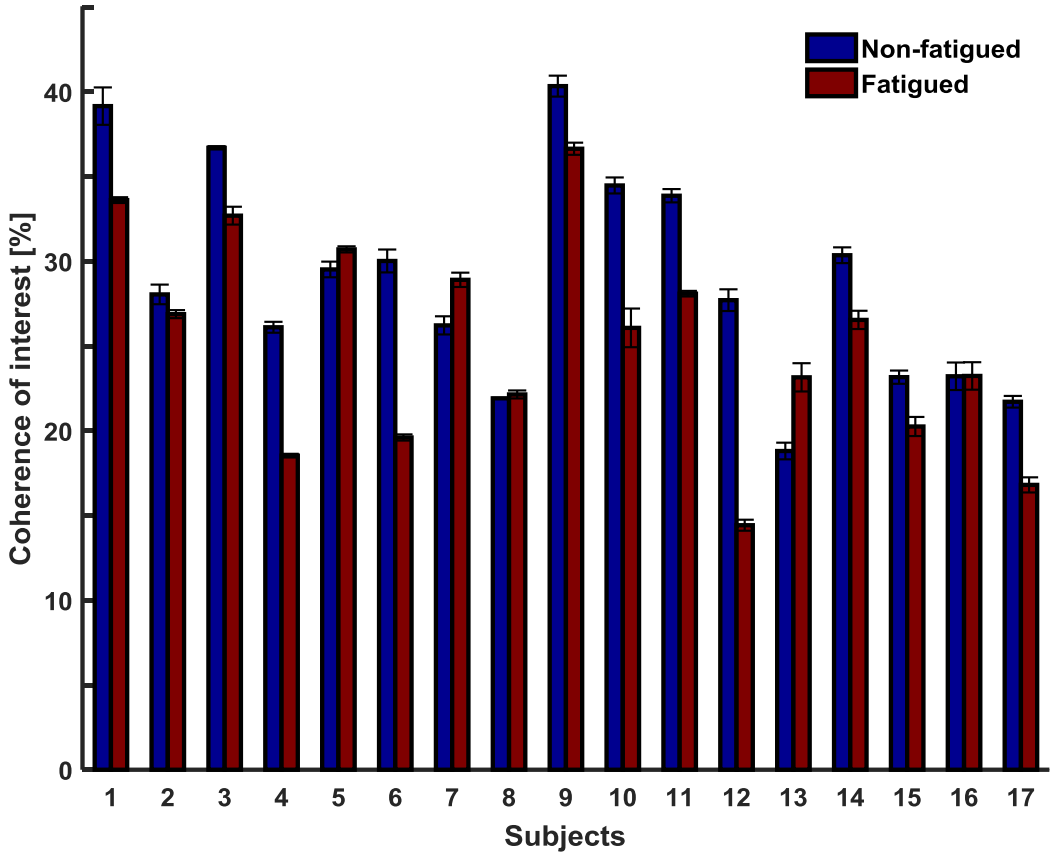

Figure 4-4. Normalized coherence of interest (10 – 100 Hz) ± SEM for the first 60 EMG events (non-fatigued), and the last 60 EMG events (fatigued) during the cycling protocol of seventeen subjects.

The t-test showed a statistically significant difference in coherence ($p = 0.005$). This result showed that there is a significant decrease in coherence in the frequency range between 10 Hz and 100 Hz for the fatigued condition when comparing to a non-fatigue condition (Figure 4-5).

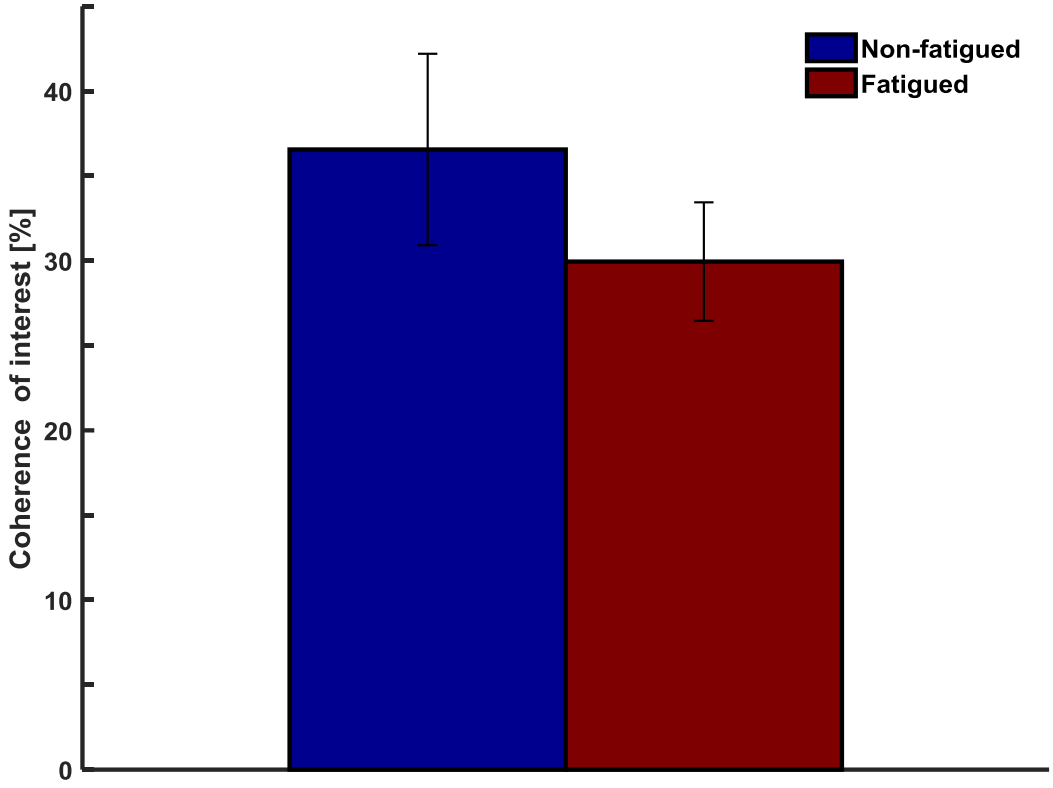

Figure 4-5. Coherence of interest for all subjects (mean ± SD). There is a significant difference ($p = 0.005$) when comparing the non-fatigued with the fatigued condition.

The histogram of the percentage of decrease in the coherence of interest showed that 13 subjects decreased, and 4 subjects increased (Figure 4-6).

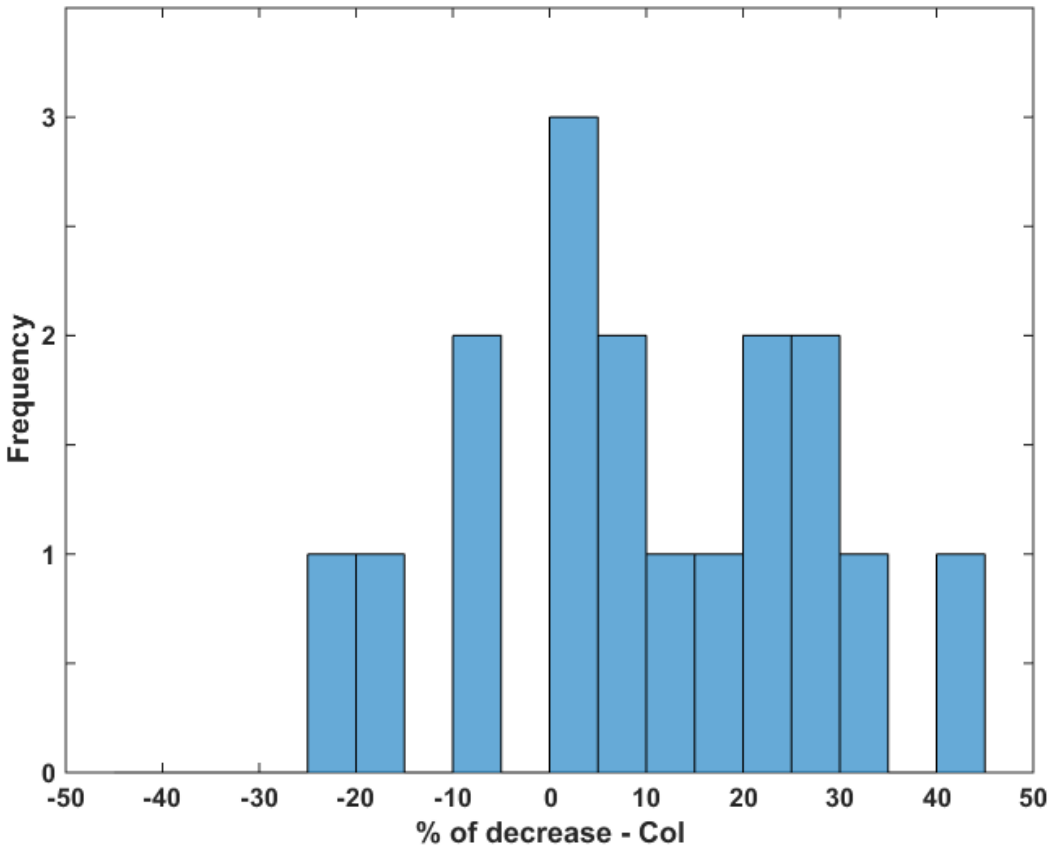

Figure 4-6. Histogram of the percentage of decrease in the mean CoI for all 17 subjects. Each bin represents 5%. Positive values refer to a decrease (13 subjects); negative values refer to an increase (4 subjects)

The results for the MDF are shown in Figure 4-7. For 14 subjects the MDF of VM decreased 11.4 ± 0.6 % (mean ± SEM), and for 7 subjects the MDF of VL 9.5 ± 0.9 % (mean ± SEM). On the other hand, for 3 subjects the MDF of VM increased 3.3 ± 1.3 % (mean ± SEM), and for 10 subjects, the MDF of VL increased 5.4 ± 0.3 % (mean ± SEM).

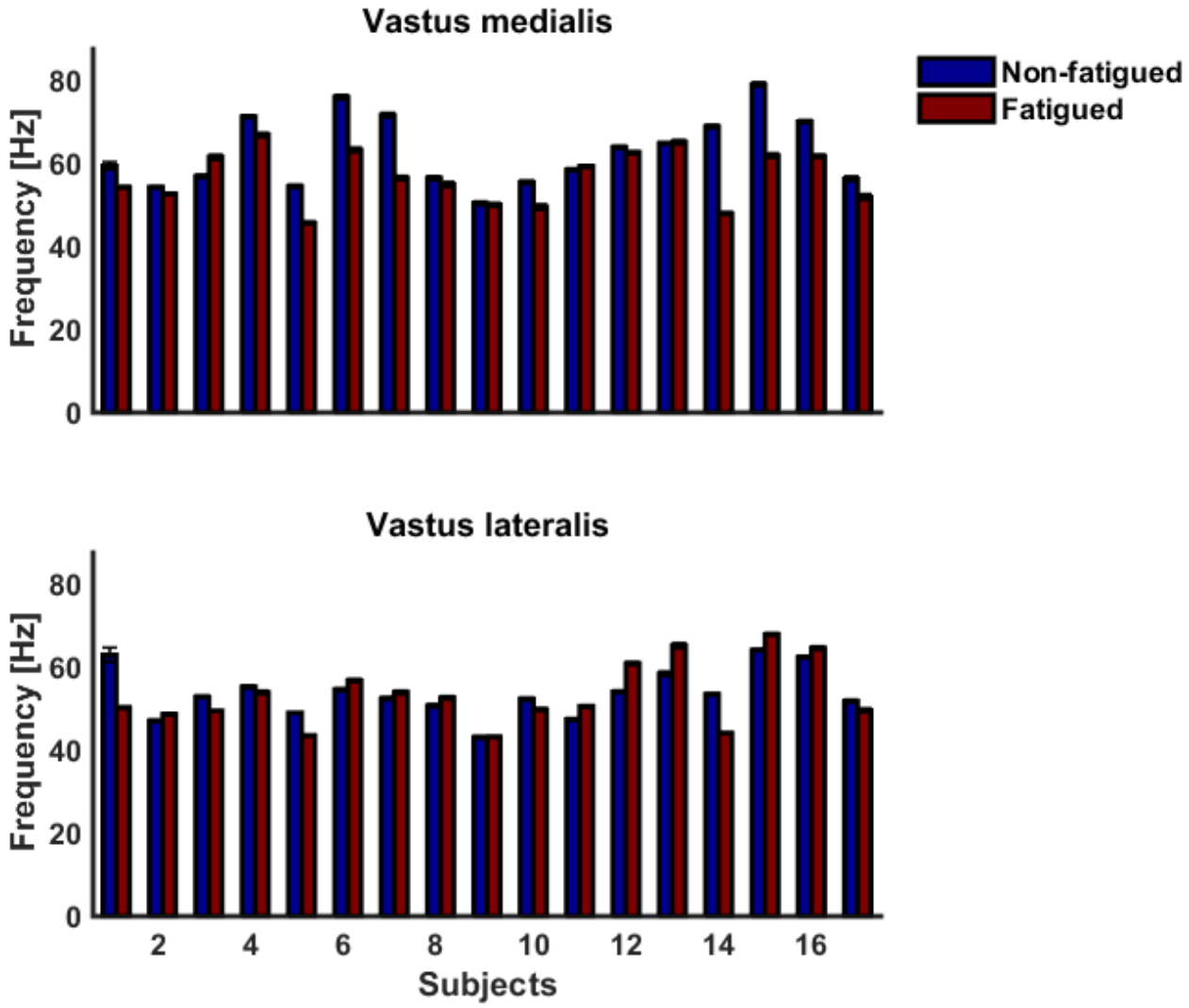

Figure 4-7. Median frequency (MDF ± SEM) of the power spectral density for VM and VL for the same data as the one used for coherence analysis.

The t-test showed no significant difference in the median frequency for the VM ($p = 0.178$) and for the VL muscle ($p = 0.556$) when comparing the non-fatigued vs. the fatigued condition (Figure 4-8).

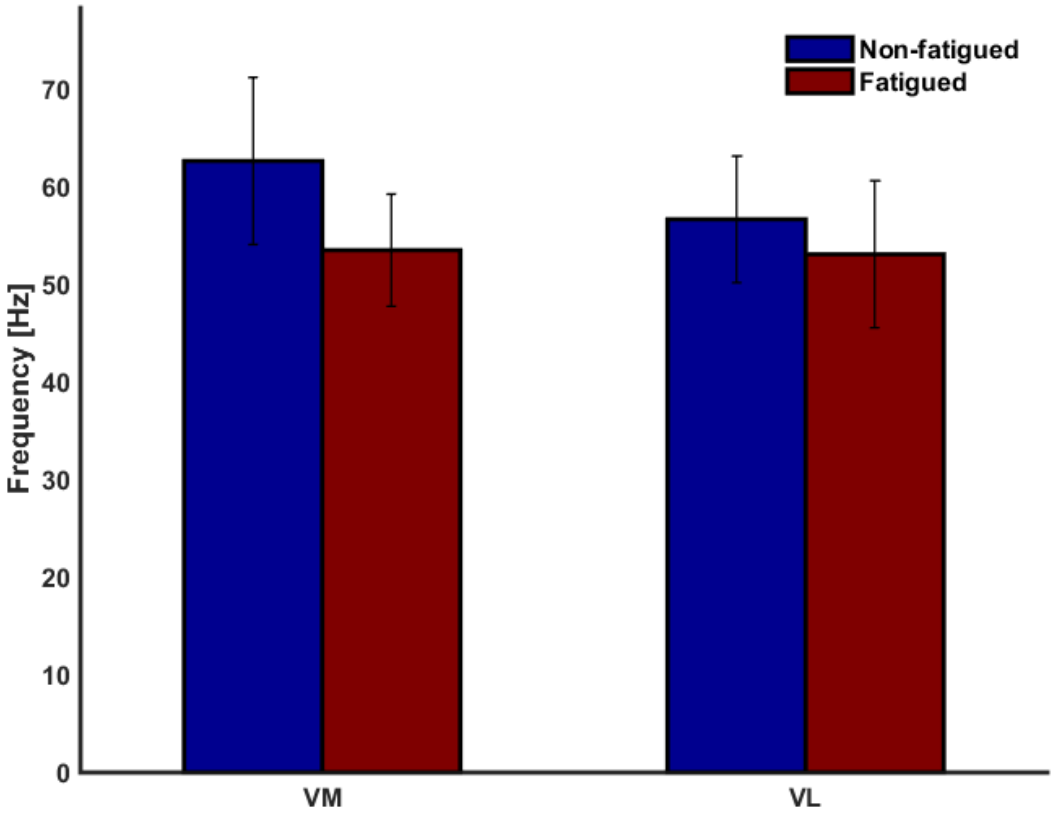

Figure 4-8. MDF of VM and VL for all subjects (mean ± SD). There is no significant difference when comparing the non-fatigued with the fatigued condition for VM ($p = 0.178$) or VL ($p = 0.556$).

The percentage of decrease of the MDF results are shown in Figure 4-9. For the VM: 14 subjects decreased, 3 subjects increased. For the VL: 7 subjects decreased, and 10 subjects increased.

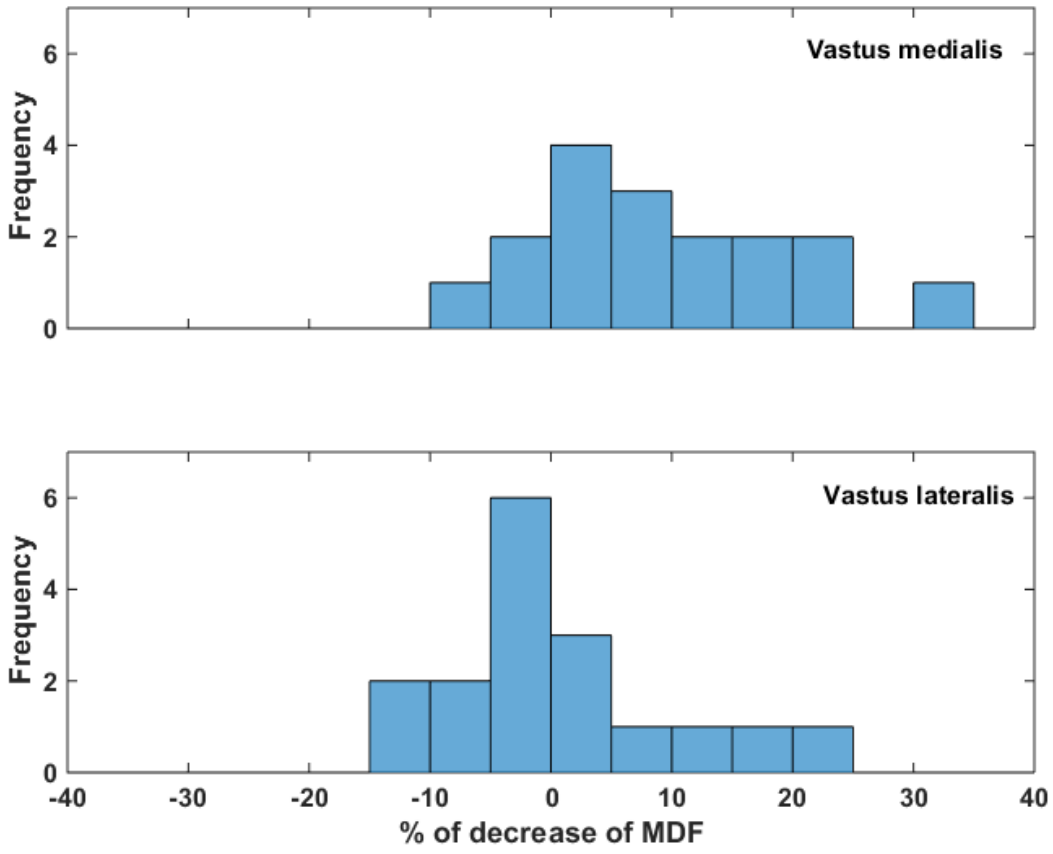

Figure 4-9. Histogram for the decrease of MDF for all subjects. Each bin represents 5%. Positive values refer to a decrease (14 for VM, 7 for VL); negative values refer to an increase (3 for VM, 10 for VL).

4.4 Discussion

The results show that there exists a significant difference for the non-fatigued versus the fatigued condition in the coherence of interest, CoI, between VL and VM during the tested cycling movements. This is in agreement with results from earlier experiments during fatiguing squat movements [5]. However, not all subjects had a decrease in coherence despite the fact that all the

subjects finished the protocol at volitional exhaustion. Four subjects showed an increase their coherence level between VL and VM. This results suggests that the decrease of the coherence of interest, CoI, with fatigue seems to be subject dependent. This subject dependent effect has also been reported in the previous study [5].

One possible reason for this result could be that those subjects who did not show a decrease in coherence might have used a different strategy to overcome fatigue. It could be that these subjects used different muscles, muscles that were not measured. Another possible explanation of this result that some subjects did not showed a decrease in the Coherence of interest (CoI), may be associated with the fact that these subjects participated in different activities for their usual exercises (e.g. basketball, soccer, weightlifting, etc.). These different activities could have a different effect in the training of the vastii muscles and thus, their coherence levels may have a range of variation under a fatiguing cycling exercise. This speculation would be in agreement with a study that looked into the motor unit synchronization of hand muscles from musicians and weightlifters. The study found that the weightlifters have increased motor unit synchronization compared to the musicians and a control population [25]. If coherence is a possible indicator of fatigue one needs to understand the factors that influence coherence to be able to use this information as a fatigue indicator. At this point in time, the knowledge is not available and these possible factors need to be further investigated.

The second major result from this study is related to the median frequency. The median frequency was calculated for the same EMG data as the coherence. There was no significant difference between the non-fatigued and the fatigue condition for the median frequency. Again, one needs to understand the factors that influence the median frequency and their relationship to fatigue. As mentioned before, the median frequency calculation, is often used in isometric

contractions [46]. There are several possible reasons for the changes in the EMG signal that lead to this decrease in the median frequency: modulation of recruitment firing rate, grouping and slowing of conduction velocity, etc. [49]. Currently, the median frequency might not be an appropriate method to assess for fatigue during dynamic activities.

The median frequency calculation only takes into account one muscle, thus, it reflects the peripheral fatigue (i.e. the fatigue of the muscle by itself). The coherence calculation looks into the common input received by two muscles, so one could assume that it reflects the central fatigue (i.e. the fatigue suffered by the central nervous system). It could possibly be that the median frequency does not show a difference in dynamic situations because the muscles were not completely fatigued; however, since the experiment seemed to be psychologically demanding for the subjects, the coherence might have shown the significant decrease because it is related to the central fatigue.

Another possibility is that the coherence calculation requires the power spectrum of both muscles. The fact that the coherence shows a decrease during a fatiguing activity while the MDF does not could be related to a limitation in the MDF calculation. Small changes in the power spectrum profile result in small changes in the MDF. However, since coherence is a correlation of both the power spectrums, a small change in the individual power spectrums profiles causes a large change in the coherence.

Another reason for the fact that the coherence of interest method, CoI, does not provide a stronger grouping of fatigued versus non-fatigued may be in the fact that the EMG signals of only two muscles were analyzed. It may be that a general method for fatigue identification needs more than one muscle pair.

4.5 Summary

In this chapter a cycling experiment was described. The experiment aimed to assess whether or not coherence between the EMG of the two vastii muscles decreases due to fatigue. The data processing to compute a coherence of interest (CoI) between 10 and $100\ Hz$ was described. The results were compared to the conventional median frequency (MDF) shift shown for isometric contractions in the literature. Our results show that the coherence level between both muscles had a significant decrease during fatigue while the MDF did not showed significant results for both muscles. This result suggests that neither coherence, nor median frequency are currently a perfect predictor for fatigue. However, for the vastii muscles, 13 out of the 17 subjects showed a decrease in coherence. There is a trend that coherence decreases with fatigue but further research should look into the subjects that showed no difference or even increased their coherence. Furthermore, it may be necessary to quantify the intermuscular coherence of more than one muscle pairs to have a general indicator of muscle fatigue for a subject.

The trend for the coherence result is in the decrease direction during fatigue; however, not all subjects showed this decrease. There are many factors that could have influenced their intermuscular coherence; it may be that those who did not showed decrease did so because their daily activities have trained their vastii muscles in a different manner and thus the intermuscular coherence behaves differently when starting to fatigue. However, this is merely a speculation and needs to be confirmed in future experiments.

This study suggests that one should look further into intermuscular coherence as an indicator of fatigue. To the author's knowledge, this is the second study that looks into intermuscular coherence with an EMG current-amplifier to assess fatigue in a dynamic situation. This methodology needs to be further explored to demonstrate its validity in different dynamic tasks.

The author speculates that a general fatigue identification method may need more than one muscle pair.

The next chapter will address the effect of a biofeedback system in the coherence between the lower limb muscles.

Chapter Five: **Intermuscular coherence modulation with visual biofeedback**

5.1 Introduction

Biofeedback is defined as the monitoring of a normally automatic bodily function in order to train someone to acquire voluntary control of that function[9]. Brain-machine interfaces (BMIs) are a great example of biofeedback systems, which are used in both experimental and clinical environments. BMIs acquire and translate raw electrical signals from the body (e.g. electroencephalography (EEG) electromyography (EMG), among others) to restore limb mobility to paralyzed subjects [50]. Another common practice of biofeedback is to use electrical signals from the muscles, detected using electromyography (EMG). This particular method has been demonstrated for the use of returning muscle function after trauma as well as other rehabilitation purposes [51]–[57]. In many cases, the use of EMG interfaces is preferred over BMIs because the EEG signals are more susceptible to external noises (e.g. crosstalk from EMG activity from facial muscles) and are more complicated to quantify.

For feature extraction of the EMG signals, many techniques have been used, including autoregressive coefficient (AR) [58], time domain statistics (TDS) [59], among others. Recently, experimenters have begun using frequency spectra as a feature extraction for biofeedback. In one experiment, participants were able to control a two-dimension cursor on a screen by monitoring frequency bands in the power spectral density (PSD) of one muscle [30]. Although some frequency analysis has been used for biofeedback systems (e.g. PSD), other methodologies such as intermuscular coherence, have not been implemented in these type of systems. Coherence is a

[9] http://www.oxforddictionaries.com/us/definition/american_english/biofeedback

frequency analysis that looks at the similarities of frequency content in two different signals [23]. In this case of intermuscular coherence, the analyzed signals are EMG signals.

It has been proposed that intermuscular coherence could be used for biofeedback [5]. This information would be helpful for the optimization of certain trainings or rehabilitation therapies that require a coherent activation of the muscles.

5.1.1 Hypothesis and purpose

This purpose of this study is: (a) to develop of a biofeedback system based on the integrated coherence between *vastus lateralis* (VL) and *vastus medialis* (VM); and (b) to determine if subjects are able to increase their intermuscular coherence with the use of such a coherence based biofeedback system.

The hypothesis for this experiments is:

Coherence between the vastii muscles will increase with the use of a visual biofeedback system during non-fatiguing leg extension movements.

5.2 Materials and methods

5.2.1 Biofeedback system design

The biofeedback system is composed of three elements: The new current-amplifier, the isolation module (both of these were described in chapter 2), and the biofeedback software.

5.2.2 Biofeedback software

The biofeedback software was designed using Matlab™ 2016b (Mathworks Inc. Natick, MA, USA). The software was composed of a graphical user interface to show the user their

normalized coherence of interest (CoI) for biofeedback (described in the following section), and the processing algorithms. The processing algorithms detected the muscle activation time and calculated coherence for the determined time period (using the same methodology described in chapter 4). The flow diagram of the software is shown in Figure 5-1.

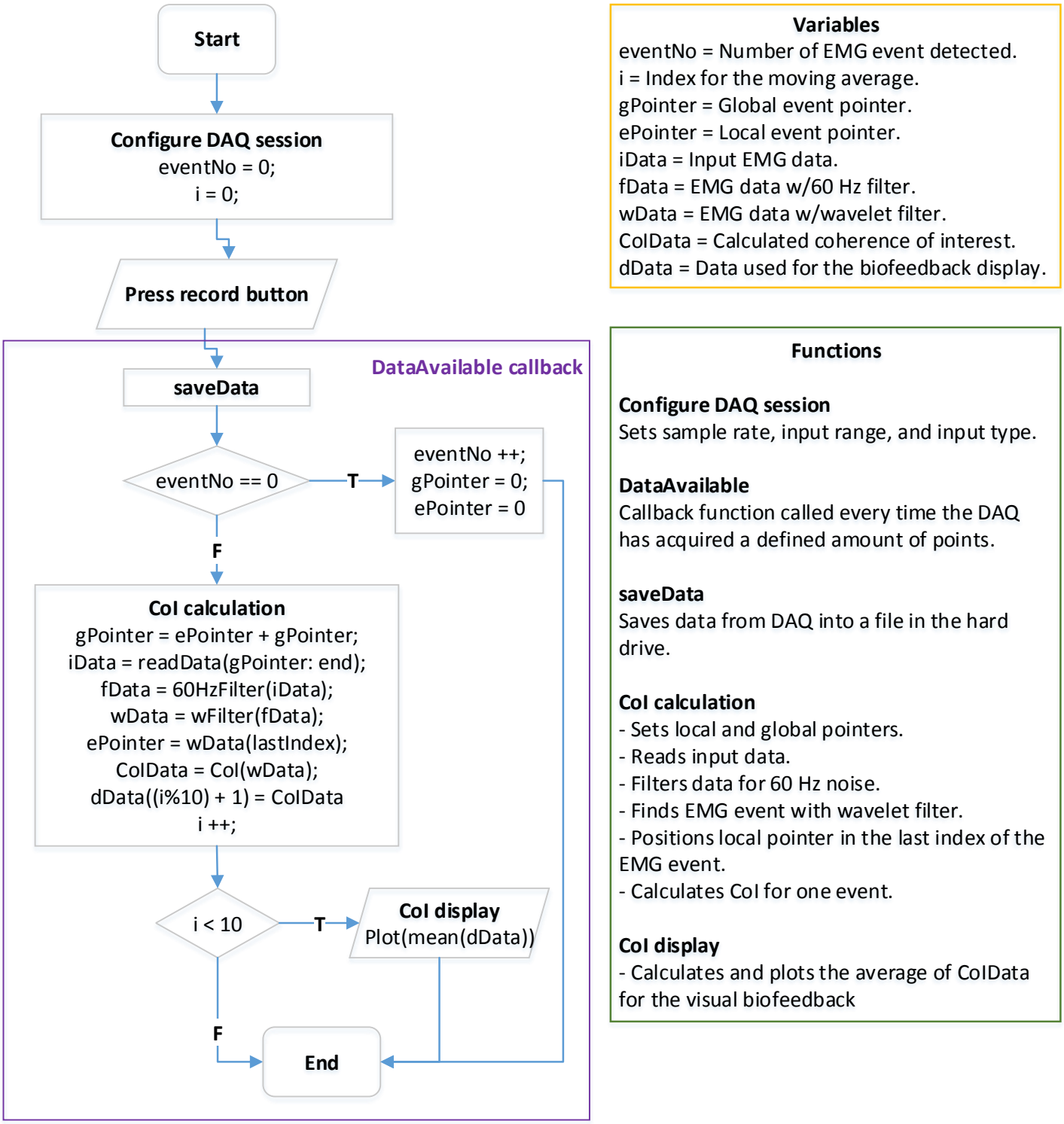

Figure 5-1. Detailed flow diagram for the biofeedback software.

The software relies on the *DataAvailable* callback. This callback allows to execute the desired functions when a specified amount of data is acquired in the data acquisition card (DAQ). For the *DataAvailable* callback, 2400 data points were chosen, the equivalent to one second of data (i.e. sample rate = 2400 Hz). Thus, every second the data sampled in the previous second is available for further analysis. One second of data was chosen for the *DataAvailable* callback because for this experiment, muscle activation occurs in bursts with a frequency of $\sim 1\ Hz$.

5.2.3 Functions

For the 2400 data points available for processing, the following functions take place in the same order as presented in this document.

5.2.3.1 Save data function

The first operation after the *DataAvailable* callback is the *saveData* function; this function appends the acquired data to a file. The saved data includes the EMG and time data as column vectors. The data saving process is important to ensure that the raw data is always stored.

Since the muscle activation can occur at any time within one second of data acquisition; during the first *DataAvailable* callback, the data is stored and no further processing takes place. This process ensures that the second time the *DataAvailable* callback occurs, at least one full muscle activation is recorded.

5.2.3.2 Coherence of Interest (CoI) calculation

After the data has been saved, the coherence of interest (i.e. the normalized integrated coherence between $10 - 200\ Hz$) is calculated (as defined in section 5.2.5). The frequency bands

were selected after a pilot study with one subject. The subject performed the same protocol later described in this chapter. The coherence for the simultaneous muscle activations (coherence), as well as the coherence for non-simultaneous muscle activations (baseline) was calculated for one trial of the subject (Figure 5-2). The calculated coherence decreases to values close to baseline at frequencies higher than 200 Hz, thus, the upper frequency limit was chosen to be 200 Hz. The limit for low frequencies, 10 Hz, was chosen according because most of the EMG frequency power is located between 10 to 250 Hz [1].

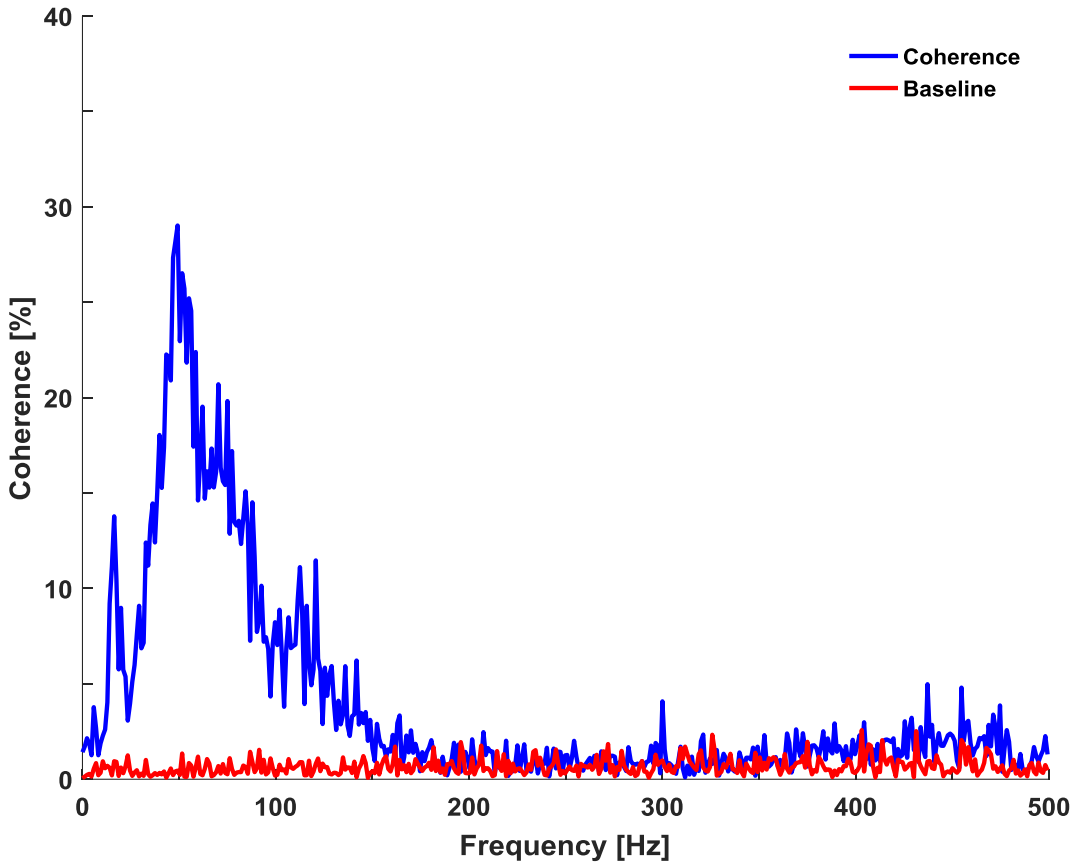

Figure 5-2. Coherence (blue) and baseline (red) for one trial of one subject. Coherence values decrease to baseline levels for frequencies higher than 200 Hz.

For the event detection algorithm, bursts of EMG activity were detected using event pointers; this makes the process more efficient by reading only a portion of the raw data file every time the DataAvailable callback occurs. There were two event pointers that were used, the first is a local pointer (ePointer), used to determine the last index of the EMG activity for the current *DataAvailable* callback; the second is a global pointer (gPointer), which was used to determine the last index of the EMG activity for the saved data file. For the first time that the *CoI calculation* function is called (i.e. the second time the *DataAvailable* callback occurs), *ePointer* and *gPointer* are set to zero.

After the data is read, the signal is filtered with a 60 Hz line-averaging filter (*60HzFilter* function). This filter eliminates the 60 Hz noise without inducing a notch effect in the signal or altering its phase [2].

The next filter is a wavelet based filter (*wFilter* function) this filter is used to determine the activation time of the EMG signal (refer to chapter 4 for a more detailed explanation of this filter). A wavelet transform is used to find the envelope of the EMG signal. Then, after the first local peak is identified, a window of 2^{10} (1024) data points were taken both before and after the peak. Thus, a total of 2^{11} (2048) points are used for further analysis; this data is labeled as *wData*. This amount of data was chosen because it closely approaches the time that the muscle is active during the protocol movement; this was calculated with the pilot data. The local pointer (*ePointer*) is then re-located to the index of the last point in the previously mentioned bin.

5.2.3.3 Coherence of interest display

The previously selected data (*wData*) is stored in the *cData* array. The *cData* array stores the data for up to ten EMG activations that will be used for the coherence calculation. The second

decision block (Figure 5-1) ensures that the *cData* array has the ten values for the coherence calculation. If the index variable (*i*) is greater than ten, the coherence is calculated for the elements stored in the *cData* array and displayed to the user in the graphical user interface (GUI).

The last decision block is used to arrange the elements of the *cData* array to serve as a moving average. As an example, once the element eleven is calculated, element one is discarded and element eleven is appended to the *cData* array. This process ensures that only the last ten EMG activations are used for the coherence calculation. This averaging also induces some limitations that will be later discussed.

The data displayed to the user is a horizontal line that represents the mean of the coherence of interest (i.e. percentage of the area under the curve of the coherence between 10 – 200 Hz).

5.2.4 Protocol

Ten healthy male subjects (26 ± 2.3 YO) were recruited for the experiment. EMG activity of the VL and VM muscles was acquired as described in chapter 4. The subjects were sitting on a table with both of their legs hanging free (Figure 5-3). Subjects were instructed to perform leg extensions only with their right leg at a rate of 0.5 Hz. A digital metronome was used to instruct the subjects the timing to perform the leg extensions. The metronome was set to 60 bpm and was configured to perform two distinct sounds; the first sound marks when the subject must have his leg at a 90° knee angle (Figure 5-3.a or c), and the second sound instructs the subject to have his leg at a 0° knee angle (Figure 5-3.b). The subjects performed six trials, each lasting three minutes. The test consisted of three control trials (without biofeedback) and three biofeedback trials, the order of which was randomized to avoid any biasing effects. After each trial the subjects were

given a two-minute period to rest to stand or walk to avoid numbness in their legs due to the sitting position.

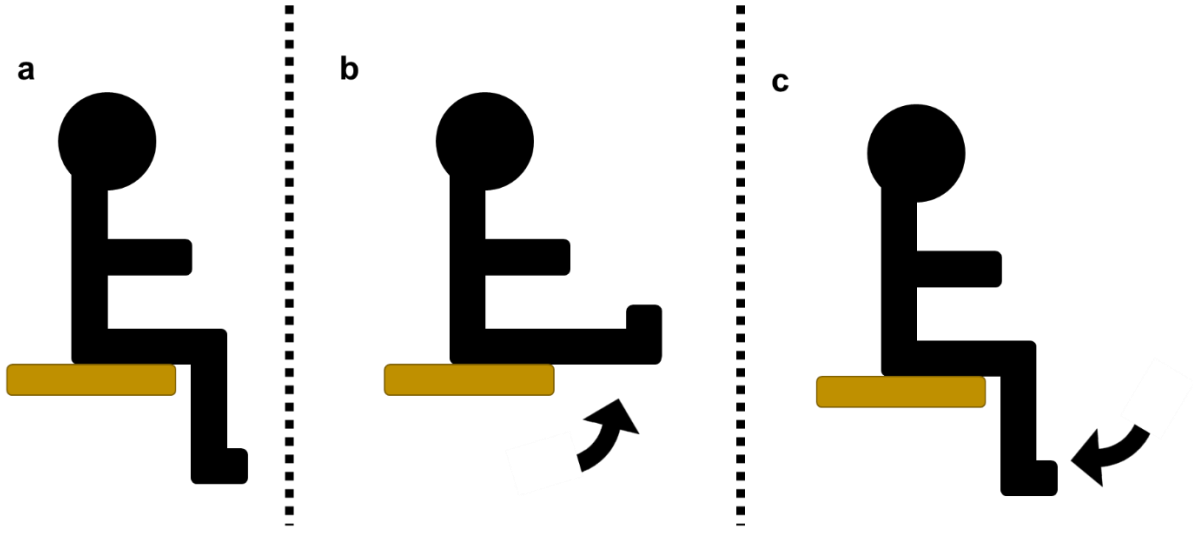

Figure 5-3. Illustration of the leg extension protocol. (a) starting position (90° knee angle). (b) Leg extension on the first metronome sound (0° knee angle). (c) Return to starting position on the second metronome cue (back down to 90^{o}).

5.2.5 Data processing

Following a similar methodology to the one explained in chapter 4, a coherence of interest computation was performed on the EMG signals from the vastii muscles. The coherence of interest, CoI, was calculated using all the muscle activations encountered. The trials have 84 ± 3 (mean ± SEM) muscle activations, this variation exists because the subjects could miss the rhythm of the metronome and compensate by performing less muscle activations until they synchronized the movement with the metronome again. The three trials for each condition are reported as mean ± SEM for all subjects.

For the statistical analysis, the mean coherence of interest for each condition was taken. A paired samples t-test was used to determine differences between the control and the biofeedback condition.

5.3 Results

All subjects showed increased their level of coherence when comparing the biofeedback to the control condition. (Figure 5-4). The coherence level increased 25 ± 4.2 % (mean ± SEM).

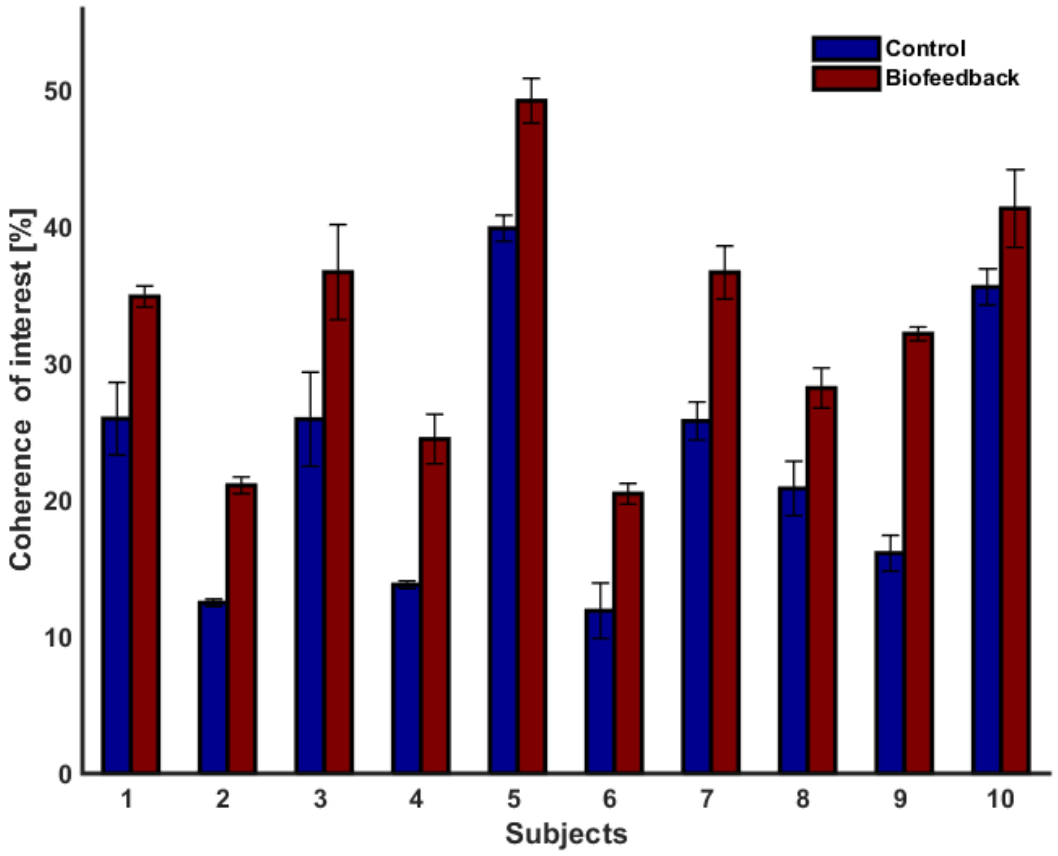

Figure 5-4. Normalized mean coherence of interest (10 – 200 Hz) ± SEM of the three control and the three biofeedback trials of all subjects.

The t-test showed a statistically significant difference in coherence ($p < 0.001$). This result showed that there is a significant increase in coherence in the frequency range between 10 Hz and 200 Hz for the biofeedback condition when compared to the control (Figure 5-5).

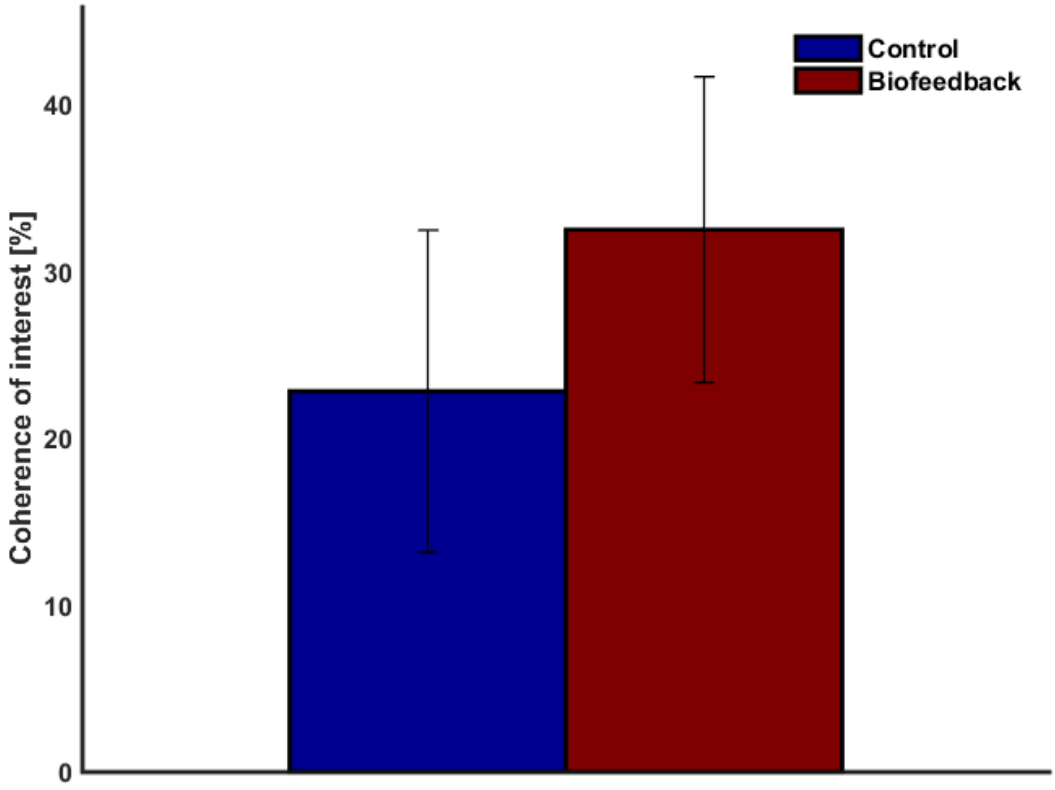

Figure 5-5. Coherence of interest for all subjects (mean ± SD). There is a significant difference ($p < 0.001$) when comparing the biofeedback to the control condition.

5.4 Discussion

The results showed a significant increase in the intermuscular coherence when comparing the control versus the biofeedback conditions. This suggests that it is possible to increase the level

of intermuscular coherence when a visual biofeedback is provided. Previous research speculates that the intermuscular coherence is controlled by the central nervous system by modulating the common input to the motor units of the individual muscles [4]. Our findings suggest that one is able to change this common input signals sent from the brain. This finding suggest that the coherence biofeedback a could be used as a tool to train muscles that require a certain level of common input to perform a movement. A good example for this type of training is related to the results found in chapter 4; in chapter 4 it was shown that for dynamic situations, coherence seems to be a good indicator of fatigue. Athletes that are interested in training programs to enhance endurance (i.e. resist longer without fatigue), could benefit from a biofeedback training that allows them to train their muscles to exercise longer without fatigue.

Additionally, this type of biofeedback systems could be used to enhance the control over robotic prosthesis by using the intermuscular coherence of residual limbs as input to the prosthesis. Human movements have shown to require a certain level of MU synchronization [25], [60]–[62]; this synchronization translates into intermuscular coherence [2]–[5]. It makes sense that intermuscular coherence could be used as the instructions to control a prosthesis, because it seems that for dynamic contractions, a certain level or synchronization (or coherence) is required.

However, the results presented here are the first indication that one can change the intermuscular coherence with the use of a biofeedback system. The examples presented are pure speculation of future work that could result from this type of biofeedback systems.

5.4.1 Limitations

One limitation for the results of this study is the control of the movement. The subjects were performing the same movement based on the metronome sounds. However, the velocity of the leg

extension movement was not controlled. Thus, the manner in which this movement was performed over time could have been different. The subjects were instructed to have their leg at a certain position for each beat of the metronome and to keep the movement direction consistent, however, the velocity at which they extended their leg was not controlled, nor was it measured. A change in movement speed, for instance, could affect the level of coherence because the task performed was not exactly the same as the control test. This is in accordance to previous research that shows that the coherence level is different for different types of squats [4].

Another limitation was the fact that, for the visual biofeedback, the coherence was calculated as an average of several EMG activations. This created frustration and confusion among the subjects because, if one of the EMG activations had a high level of coherence this would increase the visual biofeedback substantially. However, once the moving average process removed this high coherence EMG activation, the blue line would decrease and the subject could get confused by the fact that his contraction was not giving the desired level of coherence. Each subject was informed of how the software performed the coherence calculation, particularly, of how a drop in coherence could occur; nevertheless, there was a clear frustration of the subjects from this situation.

5.5 Summary

The aim of this project was to develop the biofeedback system and test if such system could improve the coherence of the vastii muscles. The system consisted of a EMG current-amplifier, an isolation module (for measuring multiple muscles simultaneously), and a biofeedback software.

The results showed that, with the visual biofeedback, the users were able to increase their intermuscular coherence during a non-fatiguing leg extension movement. This increase in coherence might be explained assuming that the users changed their strategies for the leg extension

movements. These changes would increase the common input to the motor units of the vastii muscles and increase the level of intermuscular coherence.

This study was primarily interested in the immediate increase of coherence with the use of a biofeedback system. It would be of interest to expand the scope of this research by examining the long-term effect of biofeedback by training with a similar system to see if the coherence changes can persist over time.

To the authors' knowledge, this study is the first attempt to create a biofeedback system based on intermuscular coherence. EMG biofeedback has been proven to be effective in motor impairment rehabilitation (e.g. stroke, cerebral palsy), as well as motor restoration with the use of electronic prostheses [51], [56], [57]. Further research should look at improving the current system by providing a biofeedback per muscle contraction rather than an average, as well as additional applications for it. The use of an intermuscular coherence biofeedback system could further improve sports training or rehabilitation scenarios that require a coherent activation of muscles in the same functional group.

Chapter Six: **Conclusions**

6.1 Hardware development

Electromyography (EMG), the methodology to record electrical activity generated by the muscles, has been measured in the same manner for many years [63]. The instrumentation to measure EMG is usually a bipolar instrumentation amplifier with surface electrodes (i.e. electrodes that are connected to the surface of the skin) [1]. It has been proposed that this methodology might not be the most appropriate to measure pennate muscles (e.g. vastus lateralis and vastus medialis) because of the loss of frequency information of the EMG signal due to the bipolar instrumentation amplifiers [2]. Thus, a new methodology that relies in amplifying currents instead of potentials was proposed [2].

In this thesis, the development of a new version of the previously proposed current-amplifier [2] is described and discussed. The originally designed current based method lacked active components for the filters used. The implemented filters were of a first order (i.e. with a 20 dB loss per decade); thus, the filters were insufficient to provide a flat frequency response for the frequency-range of interest (10 to 500 Hz) [1]. The new amplifier was designed with higher order filters that allow for a flat frequency response in the frequencies of interest. The implementation of the higher order filters also improved the rejection of drift currents caused by the interaction between the skin and the electrodes.

In addition to the design of the new amplifier, an isolation module was designed. The original amplifier had a crosstalk issue that occurred when more than one muscle was measured at the same time. Previous work described the origin of this crosstalk [5]. An isolation module was designed to overcome the crosstalk issue. The isolation module works by providing separate power

supplies to the multiple amplifiers. The outputs of the amplifiers are then combined to a single supply amplifier with an optical coupling device to be digitized.

The new current-amplifier, as well as the isolation module were built on prototype boards and tested to ensure their optimal performance. After testing, both devices were then built on a printed circuit board to be used in further experiments.

Future research should focus in the improvement of the new current-amplifier. The new design could be implemented in individual wireless modules that remove the isolation module and allow for research applications that require free mobility of the subjects. Improvements for rejecting common mode noise (e.g. noise from the power lines) could also increase the research possibilities by allowing to use the amplifier near dynamometers or other equipment that generates electrical noise.

6.2 Fatigue and intermuscular coherence

An experiment to measure the EMG activity of the vastus lateralis (VL) and vastus medialis (VM) during a fatiguing cycle protocol was conducted. The acquired data was used to calculate the intermuscular coherence (i.e. correlation between the frequency information of two muscles) for a fatigued and a non-fatigued condition. The results show a trend for a decrease of coherence in the fatigue condition. For the same EMG data, the median frequency (i.e. the frequency at which the EMG power spectrum is divided into two regions with equal power [45]) was calculated. The median frequency did not show any significant differences for VL or VM for the fatigue condition.

Our results suggest that currently, neither coherence nor the median frequency are a good indicators of fatigue. It is speculated that the fact that coherence did not decrease for all the subjects is related to the fact that other muscles (which were not measured) influenced the strategies used

by the body to overcome fatigue. The subjects reported to do different activities for their regular exercises (e.g. basketball, soccer, weightlifting). The fact that the subjects performed different activities, could have influenced how their muscles behave when becoming fatigued. This is in accordance with previous studies that show different levels motor unit synchronization for strength-trained and skilled-trained subjects [25].

Because of the trend for the coherence decrease (13 of the 17 subjects showed a decrease) it is speculated that coherence has the potential to be an indicator for fatigue. However, further research is needed involving other dynamic situations and/or more muscle pairs to determine if intermuscular coherence could be used as an indicator of fatigue.

6.3 Biofeedback and coherence

A biofeedback system was developed. The system integrated the previously mentioned new current-amplifier, the isolation module, and a visual biofeedback software. A study to show if a subject could increase the level of intermuscular coherence between VL and VM was conducted. The study consisted of a leg extension protocol with randomized trials for a control (no biofeedback) and a biofeedback condition. The results showed an increase of the intermuscular coherence for the trials with the biofeedback for all test subjects.

To the best of the author's knowledge, this is the first study that looks at a biofeedback system that is based on intermuscular coherence. Further research should focus on the implementation of a training program to assess the long term effects in intermuscular coherence with the use of such biofeedback system. If coherence can be improved with the implementation of a training program, a biofeedback system could be useful for rehabilitation or sports activities where the user is interested in improving the coherence of certain muscles in a functional group.

References

[1] P. Konrad, “The abc of emg,” *A Pract. Introd. to Kinesiol. Electromyogr.*, vol. 1, no. April, pp. 30–35, 2005.

[2] V. von Tscharner, C. Maurer, F. Ruf, and B. M. Nigg, “Comparison of electromyographic signals from monopolar current and potential amplifiers derived from a penniform muscle, the gastrocnemius medialis,” *J. Electromyogr. Kinesiol.*, vol. 23, no. 5, pp. 1044–1051, 2013.

[3] V. von Tscharner, C. Maurer, and B. M. Nigg M., “Correlations and coherence of monopolar EMG-currents of the medial gastrocnemius muscle in proximal and distal compartments,” *Front. Physiol.*, vol. 5, no. June, pp. 1–9, 2014.

[4] M. Mohr, M. Nann, V. Von Tscharner, B. Eskofier, and B. M. Nigg, “Task-dependent intermuscular motor unit synchronization between medial and lateral Vastii muscles during dynamic and isometric squats,” *PLoS One*, vol. 10, no. 11, pp. 1–18, 2015.

[5] M. Nann, “Synchronization of monopolar EMG-currents between the vastii muscles during fatiguing squat movements Masters Thesis in Computer Science,” 2014.

[6] R. Merletti, P. A. Parker, R. Merletti;, and P. A. Parker, *Electromyography: physiology, engineering, and non-invasive applications*, vol. 11, no. 9. John Wiley & Sons, 2004.

[7] A. C. Guyton and J. E. Hall, *Textbook of medical physiology*. Elsevier Health Sciences, 2006.

[8] E. Marieb and K. Hoehn, *Human anatomy & physiology*. Pearson, 2013.

[9] F. Huxley and R. M. Simmons, “Proposed mechanisms of force generation in striated muscle,” *Nature*, vol. 233, pp. 533–538, 1971.

[10] G. Kamen and D. A. Gabriel, “Essential of Electromyography,” in *Essentials of*

Electromyography, Human Kinetics, 2010, p. 265.

[11] G. S. Kasman, J. R. Cram, and S. L. Wolf, *Clinical Applications in Surface Electromyography: Chronic Musculoskeletal Pain*. Aspen, 1998.

[12] J. Perry, *GAIT Pathological Function*. Slack, 1992.

[13] X. Ramus, "Transimpedance Considerations for High-Speed Amplifiers. Texas Instruments. Application Report," no. November, p. 9, 2009.

[14] R. Mancini and B. Carter, "Op amps for everyone," *Newness*, no. September, 2009.

[15] X. S. U. Manual, "DAQ X Series," *Program*, no. December, 2010.

[16] W. M. Leach, "Fundamentals of Low-Noise Analog Circuit Design," *Proc. IEEE*, vol. 82, no. 10, pp. 1515–1538, 1994.

[17] C. D. Motchenbacher, J. A. (Joseph A. Connelly, and C. D. Motchenbacher, *Low-noise electronic system design*. Wiley, 1993.

[18] D. K. Schroder, *Semiconductor Material and Device Characterization: Third Edition*. John Wiley and Sons, 2005.

[19] R. L. Lieber and J. Friden, "Functional and clinical significance of skeletal muscle architecture," *Muscle Nerve*, vol. 23, no. 11, pp. 1647–1666, 2000.

[20] R. Merletti and L. R. Lo Conte, "Surface EMG signal processing during isometric contractions," *J. Electromyogr. Kinesiol.*, vol. 7, no. 4, pp. 241–250, Dec. 1997.

[21] N. A. Dimitrova, A. G. Dimitrov, and G. V. Dimitrov, "Calculation of extracellular potentials produced by an inclined muscle fibre at a rectangular plate electrode," *Med. Eng. Phys.*, vol. 21, no. 8, pp. 583–588, 1999.

[22] L. Mesin, R. Merletti, and T. M. M. Vieira, "Insights gained into the interpretation of surface electromyograms from the gastrocnemius muscles: A simulation study," *J.*

Biomech., vol. 44, no. 6, pp. 1096–1103, Apr. 2011.

[23] V. von Tscharner and M. Barandun, "Wavelet based correlation and coherence analysis reveals frequency dependent motor unit conduction velocity of the abductor pollicis brevis muscle," *J. Electromyogr. Kinesiol.*, vol. 20, no. 6, pp. 1088–1096, 2010.

[24] S. F. Farmer, F. D. Bremner, D. M. Halliday, J. R. Rosenberg, and J. a Stephens, "The frequency content of common synaptic inputs to motoneurones studied during voluntary isometric contraction in man.," *Physiology*, pp. 127–155, 1993.

[25] J. G. Semmler, M. V Sale, F. G. Meyer, M. A. Nordstrom, and J. G. Semmler, "Motor-unit coherence and its relation with synchrony are influenced by training," *J. Neurophysiol.*, vol. 92, no. 6, pp. 3320–3331, 2004.

[26] T. W. Boonstra and M. Breakspear, "Neural mechanisms of intermuscular coherence: implications for the rectification of surface electromyography," *J. Neurophysiol.*, vol. 107, no. 3, pp. 796–807, 2012.

[27] R. H. T. Edwards, "Biochemical bases of fatigue in exercise performance: Catastrophe theory of muscular fatigue," in *International series on sport sciences*, 1983, pp. 3–28.

[28] N. A. Kamaruddin, P. I. Khalid, and A. Z. Shaameri, "The Use of Surface Electromyography in Muscle Fatigue Assessments–A Review," *J. Teknol.*, vol. 74, no. 6, pp. 119–124, 2015.

[29] J. Weisz, B. Shababo, L. Dong, and P. K. Allen, "Grasping with Your Face," Springer International Publishing, 2013, pp. 435–448.

[30] C. Perez-Maldonado, A. S. Wexler, and S. S. Joshi, "Two-dimensional cursor-to-target control from single muscle site sEMG signals," *IEEE Trans. Neural Syst. Rehabil. Eng.*, vol. 18, no. 2, pp. 203–209, Apr. 2010.

[31] J. Weisz, A. G. Barszap, S. S. Joshi, and P. K. Allen, “Single muscle site sEMG interface for assistive grasping,” *IEEE Int. Conf. Intell. Robot. Syst.*, no. Iros, pp. 2172–2178, 2014.

[32] A. Malvino and D. J. Bates, *ELECTRONIC PRINCIPLES*. McGraw-Hill Education, 2016.

[33] V. Semiconductors, “Designing Linear Amplifiers Using the IL300 Optocoupler Vishay Semiconductors.”

[34] R. Mellor and P. Hodges, “Motor unit synchronization between medial and lateral vasti muscles,” *Clin. Neurophysiol.*, vol. 116, no. 7, pp. 1585–1595, Jul. 2005.

[35] N. C. Chester and W. K. Durfee, “Surface EMG as a fatigue indicator during FES-induced isometric muscle contractions,” *J. Electromyogr. Kinesiol.*, vol. 7, no. 1, pp. 27–37, 1997.

[36] P. Bonato, G. R. Ebenbichler, S. H. Roy, S. Lehr, M. Posch, J. Kollmitzer, and U. Della Croce, “Muscle fatigue and fatigue-related biomechanical changes during a cyclic lifting task,” *Spine (Phila Pa 1976)*, vol. 28, no. 16, pp. 1810–1820, 2003.

[37] G. R. Ebenbichler, P. Bonato, S. H. Roy, S. Lehr, M. Posch, J. Kollmitzer, and U. Della Croce, “Reliability of EMG time-frequency measures of fatigue during repetitive lifting.,” *Med. Sci. Sports Exerc.*, vol. 34, no. 8, pp. 1316–1323, 2002.

[38] M. Iguchi, K. Baldwin, C. Boeyink, C. Engle, M. Kehoe, A. Ganju, A. J. Messaros, and R. K. Shields, “Low frequency fatigue in human quadriceps is fatigue dependent and not task dependent,” *J. Electromyogr. Kinesiol.*, vol. 18, no. 2, pp. 308–316, 2008.

[39] P. Bonato, S. H. Roy, M. Knaflitz, and C. J. De Luca, “Time frequency parameters of the surface myoelectric signal for assessing muscle fatigue during cyclic dynamic contractions,” *IEEE Trans. Biomed. Eng.*, vol. 48, no. 7, pp. 745–753, 2001.

[40] A. Georgakis, L. K. Stergioulas, and G. Giakas, “Fatigue analysis of the surface EMG signal in isometric constant force contractions using the averaged instantaneous

frequency," *IEEE Trans. Biomed. Eng.*, vol. 50, no. 2, pp. 262–265, 2003.

[41] M. Bilodeau, S. Schindler-Ivens, D. M. Williams, R. Chandran, and S. S. Sharma, "EMG frequency content changes with increasing force and during fatigue in the quadriceps femoris muscle of men and women," *J. Electromyogr. Kinesiol.*, vol. 13, no. 1, pp. 83–92, 2003.

[42] A. F. Mannion and P. Dolan, "Electromyographic median frequency changes during isometric contraction of the back extensors to fatigue," *Spine*, vol. 19, no. 11. pp. 1223–1229, 1994.

[43] J. P. Braakhekke, D. F. Stegeman, and E. M. G. Joosten, "Increase in median power frequency of the myoelectric signal in pathological fatigue," *Electroencephalogr. Clin. Neurophysiol.*, vol. 73, no. 2, pp. 151–156, 1989.

[44] J. B. Pitcher and T. S. Miles, "Influence of Muscle Blood Flow on Fatigue During Intermittent Human Hand-Grip Exercise and Recovery," *Clin. Exp. Pharmacol. Physiol.*, vol. 24, no. 7, pp. 471–476, 1997.

[45] A. Phinyomark, P. Phukpattaranont, and C. Limsakul, "Feature reduction and selection for EMG signal classification," *Expert Syst. Appl.*, vol. 39, no. 8, pp. 7420–7431, 2012.

[46] S. Thongpanja, A. Phinyomark, P. Phukpattaranont, and C. Limsakul, "Mean and median frequency of EMG signal to determine muscle force based on time dependent power spectrum," *Elektron. ir Elektrotechnika*, vol. 19, no. 3, pp. 51–56, 2013.

[47] V. Ferrer-Roca, A. Roig, P. Galilea, and J. García-López, "Influence of Saddle Height on Lower Limb Kinematics in Well-Trained Cyclists," *J. Strength Cond. Res.*, vol. 26, no. 11, pp. 3025–3029, 2012.

[48] C. R. Abbiss and P. B. Laursen, "Models to explain fatigue during prolonged endurance

cycling," *Sport. Med.*, vol. 35, no. 10, pp. 865–898, 2005.

[49] A. D. Cechetto, P. A. Parker, and R. N. Scott, "The effects of four time-varying factors on the mean frequency of a myoelectric signal," *J. Electromyogr. Kinesiol.*, vol. 11, no. 5, pp. 347–354, 2001.

[50] M. A. Lebedev and M. A. L. Nicolelis, "Brain-machine interfaces: past, present and future," *Trends Neurosci.*, vol. 29, no. 9, pp. 536–546, 2006.

[51] D. Zhang, X. Chen, S. Li, and X. Zhu, "EMG controlled multifunctional prosthetic hand: Preliminary clinical study and experimental demonstration," *2011 IEEE Int. Conf. Robot. Autom.*, no. 2, pp. 4670–4675, 2011.

[52] A. H. Arieta, R. Kato, H. Yokoi, and T. Arai, "A fMRI study of the cross-modal interaction in the brain with an adaptable EMG prosthetic hand with biofeedback," *Annu. Int. Conf. IEEE Eng. Med. Biol. - Proc.*, no. 16360118, pp. 1280–1284, 2006.

[53] A. Merlo, D. Farina, and R. Merletti, "A fast and reliable technique for muscle activity detection from surface EMG signals," *Biomed. Eng. IEEE ...*, vol. 50, no. 3, pp. 316–323, 2003.

[54] O. Fukuda, T. Tsuji, a. Ohtsuka, and M. Kaneko, "EMG-based human-robot interface for rehabilitation aid," *Proceedings. 1998 IEEE Int. Conf. Robot. Autom. (Cat. No.98CH36146)*, vol. 4, no. May, pp. 3492–3497, 1998.

[55] M. Z. Jamal, "Signal Acquisition Using Surface EMG and Circuit Design Considerations for Robotic Prosthesis," *Comput. Intell. Electromyogr. Anal. Perspect. Curr. Appl. Futur. Challengers*, pp. 427–445, 2012.

[56] L. a Nelson, "The role of biofeedback in stroke rehabilitation: past and future directions.," *Top. Stroke Rehabil.*, vol. 14, no. 4, pp. 59–66, 2007.

[57] J. V Basmajian, “Biofeedback in rehabilitation: a review of principles and practices.,” *Arch. Phys. Med. Rehabil.*, vol. 62, no. 10, pp. 469–75, Oct. 1981.

[58] Z. G. Zhang, H. T. Liu, S. C. Chan, K. D. K. Luk, and Y. Hu, “Time-dependent power spectral density estimation of surface electromyography during isometric muscle contraction: Methods and comparisons,” *J. Electromyogr. Kinesiol.*, vol. 20, no. 1, pp. 89–101, 2010.

[59] R. Boostani and M. H. Moradi, “Evaluation of the forearm EMG signal features for the control of a prosthetic hand,” *Physiol. Meas.*, vol. 24, no. 2, p. 309, May 2003.

[60] J. G. Semmler, “Motor unit synchronization and neuromuscular performance.,” *Exerc. Sport Sci. Rev.*, vol. 30, no. 1, pp. 8–14, 2002.

[61] J. C. Kline and C. J. De Luca, “Synchronization of Motor Unit Firings: An Epiphenomenon of Firing Rate Characteristics Not Common Inputs,” *J. Neurophysiol.*, no. October 2015, p. jn.00452.2015, 2015.

[62] D. Farina, “The extraction of neural strategies from the surface EMG,” *J. Appl. Physiol.*, vol. 96, no. 4, pp. 1486–1495, 2004.

[63] W. Herzog, A. C. S. Guimaraes, and Y. T. Zhang, “Emg,” *Biomech. musculo-skeletal Syst.*, pp. 308–336, 1994.

APPENDIX A: COPYRIGHT FORM 1

Title: Comparison of electromyographic signals from monopolar current and potential amplifiers derived from a penniform muscle, the gastrocnemius medialis

Author: Vinzenz von Tscharner,Christian Maurer,Florian Ruf,Benno M. Nigg

Publication: Journal of Electromyography and Kinesiology

Publisher: Elsevier

Date: October 2013

Order Completed

Thank you for your order.

This Agreement between Daniel Comaduran Marquez ("You") and Elsevier ("Elsevier") consists of your license details and the terms and conditions provided by Elsevier and Copyright Clearance Center.

Your confirmation email will contain your order number for future reference.

Get the printable license.

License Number	3957221027059
License date	Sep 27, 2016
Licensed Content Publisher	Elsevier
Licensed Content Publication	Journal of Electromyography and Kinesiology
Licensed Content Title	Comparison of electromyographic signals from monopolar current and potential amplifiers derived from a penniform muscle, the gastrocnemius medialis
Licensed Content Author	Vinzenz von Tscharner,Christian Maurer,Florian Ruf,Benno M. Nigg
Licensed Content Date	October 2013
Licensed Content Volume	23
Licensed Content Issue	5
Licensed Content Pages	8
Type of Use	reuse in a thesis/dissertation
Portion	figures/tables/illustrations
Number of figures/tables/illustrations	1
Format	electronic
Are you the author of this Elsevier article?	No
Will you be translating?	No
Order reference number	
Original figure numbers	
Title of your thesis/dissertation	DESIGN AND DEVELOPMENT OF A MULTICHANNEL CURRENT-EMG SYSTEM FOR COHERENCE ANALYSIS
Expected completion date	Sep 2016
Estimated size (number of pages)	100
Elsevier VAT number	GB 494 6272 12
Requestor Location	Daniel Comaduran Marquez 4739 Dalton Dr. NW 517 Calgary, AB T3A 2L5

APPENDIX B: COPYRIGHT FORM 2

Title: Two-Dimensional Cursor-to-Target Control From Single Muscle Site sEMG Signals
Author: Claudia Perez-Maldonado
Publication: Neural Systems and Rehabilitation Engineering, IEEE Transactions on
Publisher: IEEE
Date: 0 April 2010

Logged in as:
Daniel Comaduran Marquez
Account #:
3001066797
LOGOUT

Thesis / Dissertation Reuse

The IEEE does not require individuals working on a thesis to obtain a formal reuse license, however, you may print out this statement to be used as a permission grant:

Requirements to be followed when using any portion (e.g., figure, graph, table, or textual material) of an IEEE copyrighted paper in a thesis:

1) In the case of textual material (e.g., using short quotes or referring to the work within these papers) users must give full credit to the original source (author, paper, publication) followed by the IEEE copyright line © 2011 IEEE.
2) In the case of illustrations or tabular material, we require that the copyright line © [Year of original publication] IEEE appear prominently with each reprinted figure and/or table.
3) If a substantial portion of the original paper is to be used, and if you are not the senior author, also obtain the senior author's approval.

Requirements to be followed when using an entire IEEE copyrighted paper in a thesis:

1) The following IEEE copyright/ credit notice should be placed prominently in the references: © [year of original publication] IEEE. Reprinted, with permission, from [author names, paper title, IEEE publication title, and month/year of publication]
2) Only the accepted version of an IEEE copyrighted paper can be used when posting the paper or your thesis on-line.
3) In placing the thesis on the author's university website, please display the following message in a prominent place on the website: In reference to IEEE copyrighted material which is used with permission in this thesis, the IEEE does not endorse any of [university/educational entity's name goes here]'s products or services. Internal or personal use of this material is permitted. If interested in reprinting/republishing IEEE copyrighted material for advertising or promotional purposes or for creating new collective works for resale or redistribution, please go to http://www.ieee.org/publications_standards/publications/rights/rights_link.html to learn how to obtain a License from RightsLink.

If applicable, University Microfilms and/or ProQuest Library, or the Archives of Canada may supply single copies of the dissertation.

BACK CLOSE WINDOW